Time Constant Anomaly Detection of Thermocouples using Transient Data

by

Jose Orengo Rodriguez

A thesis submitted in partial fulfillment of the requirements for the degree of

MASTER OF SCIENCE

in

MECHANICAL ENGINEERING

UNIVERSITY OF PUERTO RICO

MAYAGÜEZ CAMPUS

2006

Approved by:

_____ _____
David Serrano, ScD Date
Member, Graduate Committee

_____ _____
Yi Jia, PhD Date
Member, Graduate Committee

_____ _____
Frederick Just, PhD Date
President, Graduate Committee

_____ _____
Pedro Resto, PhD Date
Representative of Graduate Studies

_____ _____
Paul Sundaran, PhD Date
Chairperson of the Department

Abstract

A specific methodology to detect anomalies in temperature sensors is developed in this thesis. The strategy evaluates sensor faults or variations in the transient region only by examining the signal produced by a thermocouple. The algorithm employed used a procedure in which several time derivatives are taken and filtering techniques must be present to ensure correct anomaly detection in the presence of noise.

In order to test the procedure a neural network (NN) approach that uses the data processed by the algorithm was developed. The network developed was a Radial Basis probabilistic neural network (PNN). The algorithm distinguishes anomalous sensor behavior and classifies the cause of the behavior. In almost all of the trials the estimation of the NN technique proposed was less than one percent while the greatest error was less than five percent.

Resumen

Una metodología especifica para detectar anomalies en sensors de temperature esta desarollada en esta tesis. La estrategia es evaluar las fallas en los sensores o variación en la region transiente examinando la señal producida por un thermocouple. El algoritmo empleado utilizado en el procedimeinto se aplican derivadas y se emplea una técnica de filtrar la señal contaminada por ruido para detectar la falla o anomalia corectamente.

Una red neural (NN) esta propuesta en este trabajo, para distinguir la conducta anómala en sensores de temperatura y que pueden ayudar con la clasificación de defectos se proponen. Los datos experimentales se utilizaron para entrenar la red neural propuesta. Para este caso se utilizo la estructura probabilistica Radial Basis. La literatura ofrece la evidencia substancial de técnicas o esquemas de detección y clasificación de data. La estructura de NN propuesta como sistema de detección y clasificación de daños provee un error de estimación menos del 5% de error.

Dedication

To my mother Doris and my father Edwin who never stop their support and are biggest inspiration and treasure; I love you. To God who has given a special path to follow accompanied by all the right people.

Acknowledgments

During my graduate studies at the University of Puerto Rico several people and institutions collaborated directly and indirectly with my research. Without their support it would never have been impossible to complete this work. That is why I wish to dedicate this section to recognize their support.

I want to start expressing a sincere acknowledgement to my advisor, Dr. Frederick Just-Agosto. He gave me the opportunity to perform research under his guidance and supervision. I received motivation; encouragement and support form him. I also want to thank the example, motivation, inspiration and support I received from Mr. Ezequiel. Special thanks I owe to Dr. David Serrano, Dr. Yi Jia and Dr. Gustavo Gutierrez they were always available to give support and guide in my work.

Finally without the support of Pratt & Whitney under the guidance and supervision of Dr. Ravi Rajamani and Dr. Allan Volponi none of this could be possible. Not only was I exposed to concepts in sensor and anomaly detection, their example as professionals will always be remembered; thanks a million!

At last and most important, I would like to thanks my family for their unconditional support, inspiration and love.

Contents

List of Figures

List of Tables

1 Introduction

Jet engines are complex systems that require monitoring to ensure flight safety and cost effective maintenance. Vital information such has rotor speeds, engine pressure ratios, exhaust gas temperatures, oil supply pressures, fuel consumption, vibration parameter, etc., are monitored to serve has indicators for engine performance. In addition, these parameters can be used to determine damage or imminent failure. Monitored data is usually processed in a decision algorithm, that either uses a data driven signal processing approach or a model based-diagnostics approach. Here the condition of the engine is either determined in real time or through post processing. Because sensors signals are used to evaluate the engine status for control or maintenance schedules, the ability to determine sensor anomalies is of high importance. In order to understand this idea a brief review of a gas turbine and the importance of sensor measurement follows.

1.1 Gas Turbine Review

A turbofan jet engine gas path consists of several components (Figure 1.1). The first component is the fan which is open to the outside and in a military engine provides most of the thrust by sending a vast quantity of air around the engine core. The next component is the booster, also known as the low pressure compressor (LPC), which is followed by the high pressure compressor (HPC). The HPC opens into the combustor where fuel is injected and burned. The resulting hot gas drives the high pressure turbine (HPT) and the low pressure turbine (LPT). Each of these components affects the engine's operation. The use of algorithms for improved control and knowledge about component

health enables a higher level of performance to be obtained. The state of component health involves monitoring characteristics that degrade over time: these can include efficiency, flow capacity, and seal leakage. Normally these tend to change slowly over many flights, but abrupt changes might indicate the occurrence of a sudden fault.

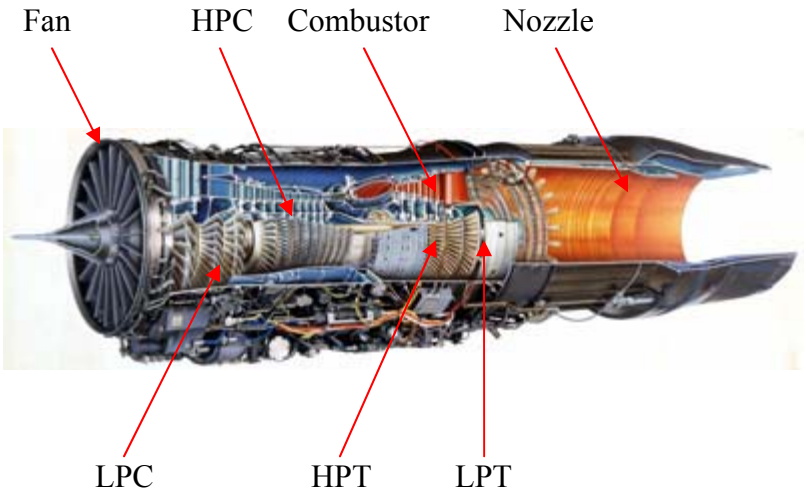

Figure 1-1: F100 Pratt & Whitney Turbofan Military Engine

In addition, jet engine gas path performance diagnostics is also performed on engines. This involves estimating the values of specific variables associated with the gas path components. Changes in these values that might indicate a fault. It is important to distinguish between the general health of the engine gas path components and sudden faults. The general health of the engine is equivalent to its level of degradation or effective age, and is the baseline from which changes are measured. In the gas path, the health condition of each component is defined by its efficiency and other parameters that slowly. In general there are not enough engine sensors available to allow estimation of

these health parameters in flight.

Thermocouples signals are often used to monitoring temperatures at various, points inside and outside the engine. The typical parameters that are recommended for monitoring a aircraft engine are temperature: inlet, outside air, exhaust gas, compressor, turbine and bleed air. Since thrust is fundamentally dependent on temperature differentials, engine temperatures are used to measure the effectiveness of engine design. For example, the temperature at the combustion chamber exit may not exceed a certain limiting value to prevent damage to the high pressure turbine. Another variable that is highly important for the safe operation of the engine is the so-called surge margin of the compressors. The surge margin describes compressors' operating range from the limit line representing the beginning of instability. Reaching this line may lead to permanent mechanical damage of the engine's components. Furthermore, the engine spool speeds may not exceed certain limiting values to ensure the mechanical integrity of the engine.

To understand how a propulsion system works and how the efficiency of engine components from thermal parameters is determined, consider the basic gas turbine cycle. The Brayton cycle is used for gas turbines only where both the compression and expansion processes take place in rotating machinery. The Brayton cycle depicts the air-standard model of a gas turbine power cycle. A simple gas turbine is comprised of three main components: a compressor, a combustor, and a turbine. According to the principle of the Brayton cycle, air is compressed in the compressor. Then mixed with fuel, and burned under constant pressure conditions in the combustor. The resulting hot gas is allowed to expand through a turbine to perform work.

A schematic of the Brayton (simple gas turbine) cycle is given in Figure 1-2. Low-pressure air is drawn into a compressor (state 1) where it is compressed to a higher pressure (state 2). Fuel is added to the compressed air and the mixture is burnt in a combustion chamber. The resulting hot gases enter the turbine (state 3) and expand to (state 4). The Brayton cycle consists of four basic processes:

a) 1 → 2: Isentropic Compression (in a compressor)

b) 2 → 3: Reversible Constant Pressure Heat Addition

c) 3 → 4: Isentropic Expansion (in a turbine)

d) 4 → 1 Reversible Constant Pressure Heat Rejection (Exhaust and Intake in the open cycle)

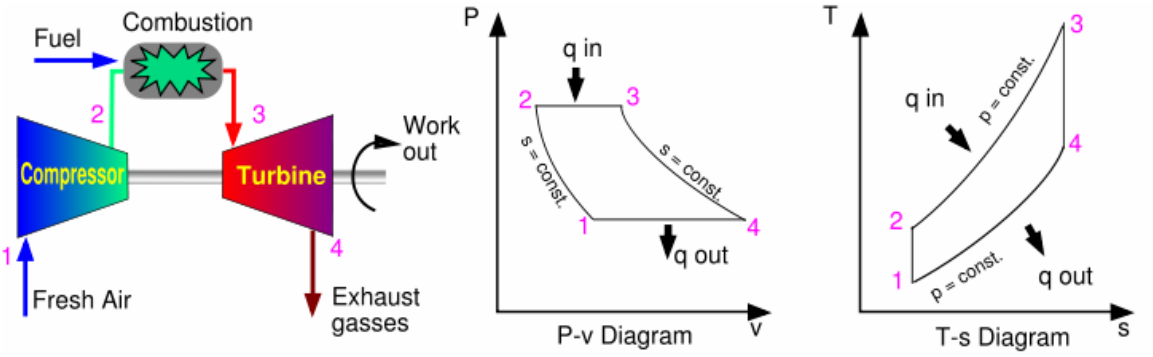

Figure 1-2: Ideal Brayton Cycle

Thermodynamics and the First Law of Thermodynamics determine the overall

energy transfer. To analyze the cycle, we need to evaluate all the states. Air standard models are very useful for this purpose and provide acceptable quantitative results for gas turbine cycles. In these models the following assumptions are made. The working fluid is air and treated as an ideal gas throughout the cycle. In addition, the combustion process is modeled as a constant-pressure heat addition. The exhaust is modeled as a constant-pressure heat rejection process.

In cold air standard (CAS) models, the specific heat of air is assumed constant (perfect gas model) at the lowest temperature in the cycle. The effect of temperature on the specific heat can be included in the analysis at a modest increase in effort. However, closed form solutions would no longer be possible.

When air table data are used to conduct an analysis involving the ideal Brayton cycle, the following relationships apply for the isentropic processes 1 → 2 and 3 → 4.

$$p_{r2} = p_{r1}\frac{P_2}{P_1} \qquad (s_1 = s_2,\ \text{air only}) \tag{1-1}$$

$$p_{r4} = p_{r3}\frac{P_4}{P_3} = p_{r3}\frac{P_1}{P_2} \tag{1-2}$$

Here the relative pressure, p_{ri}, $(i = 1, 2, 3 \text{ or } 4)$, is determined through temperature tables. Processes 1→2 and 3→4 are isentropic, and since the air flow through the heat exchanger of the ideal cycle is performed at constant pressure, $P_2 = P_3$ and $P_4 = P_1$. It follows that $P_4 / P_3 = P_1 / P_2$. This relationship has been used in writing equation 1-2.

When an ideal cycle Brayton cycle is analyzed using a cold air-standard basis, the

specific heats are assumed constant. Equation 1-1 and 1-2 are then replaced, respectively, by the following expressions:

$$T_2 = T_1\left(\frac{P_2}{P_1}\right)^{\frac{(k-1)}{k}} \qquad (s_1 = s_2,\ \text{constant k}) \qquad 1\text{-}3$$

$$T_4 = T_3\left(\frac{P_4}{P_3}\right)^{(k-1)/k} = T_3\left(\frac{P_1}{P_2}\right)^{(k-1)/k} \qquad (s_3 = s_4,\ \text{constant k}) \qquad 1\text{-}4$$

where k is the specific heat ratio, $k=c_p/c_v$.

The specific heat of each fluid should be evaluated at the linear average between its inlet and outlet temperature, $\left(\frac{T_{in}+T_{out}}{2}\right)$, for more accurate results.

The actual gas turbine cycle differs from the ideal Brayton cycle. Some pressure drop during the heat addition and heat rejection is unavoidable. Thus actual work input to the compressor will be more, than the actual work output from the turbine less because of irreversibilities. The deviation of actual compressor and turbine behavior from the idealized isentropic behavior can be accurately accounted for by utilizing the adiabatic efficiencies of the turbine and compressor defined by:

$$\eta_{TURB} = \frac{w_{TURB,a}}{w_{TURB,s}} = \frac{h_3 - h_{4,a}}{h_3 - h_{4,s}} \qquad 1\text{-}5$$

$$\eta_{COMP} = \frac{w_{COMP,s}}{w_{COMP,a}} = \frac{h_{2,s} - h_1}{h_{2,a} - h_1} \qquad 1\text{-}6$$

where states 2a and 4a are the actual exit states of the compressor and the turbine, respectively, and 2s and 4s are the corresponding states for the isentropic case.

However, if the fluid stream is assumed to be an ideal gas with constant specific heats, we may represent the enthalpy differences in terms of temperature differences by using the appropriate equation of state $(dh = c_p dT)$.

1.2 Motivation

The accuracy of measured parameters such as pressure, temperatures, rpm, and combustion flow rate to name a few can have critical influence in maintenance and control algorithms. Data is usually obtained from various types of transducers and can be classified by their dynamics behavior (zero, first or second order sensors), Dobelin, (1983). The signals from sensors are used to determine the condition of the engine in question and variations are usually treated with statistical noise estimates or models predicting the output.

Engine simulation models can play a very important role in diagnostic systems. Typically the output of the jet engine model is used to validate the sensors information. The absolute value of the difference between the actual sensor output and the model is the error; this is normally examined in a threshold scheme. The main advantages of a actual diagnostics system is its ability to distinguish anomalous behavior from normal

behavior using actual test or simulation data and help with the reliable classification of engine faults, without requiring detailed systems models. Engine simulation models can have a high cost in development and actual engine modification must either be corrected for remodeled. This thesis will focus in developing a sensor diagnostic system that is independent of the engine model. First-order sensors, specifically temperature sensors will be examined.

The results of the investigation will help classify and develop monitoring techniques that will improve the jet engine reliability and usage life. Some important benefits that will result from this research are: the development of a specific methodology to detect anomalies in temperature sensors of a particular jet engine. In addition, the model will predict engine sensor behavior in real time. Thus, this that can be implemented into algorithm tools to interpret data signals for control and maintenance scheduling.

1.3 Objectives

The main objective of this work is to develop a model for anomaly detection in temperature sensors and formulate (MATLAB-Simulink) simulation model. The work will be divided into the four areas listed below:

1. Examine the feasibility of using actual transient thermocouples data to determine the possibility of determining faults or variations in readout due to time constant variation.
2. Develop an algorithm to detect the time constant of temperature sensors during a transient temperature changes.
3. Study the effect of noise in the algorithm and select an adequate filter.
4. Apply a Neural Network technique to distinguish anomalous behavior in temperature sensors that can help with classification of faults.

2 Literature Review

Sensor validation and diagnostic processes can be performed using multiple techniques that offer advantages for detecting specific sensor failure modes. Some techniques that have been implemented with success include; trained neural networks, fuzzy logic analysis, signal auto and cross correlation, and high-pass filtering. The sensor validation and diagnostic techniques are divided in to two categories: signal processed-based and physics-based. Signal processing techniques are used for detecting and diagnosing sensor anomalies. Because physics-based techniques are developed from a-priori knowledge of the system characteristics, they can be used for sensor recovery and virtual parameter sensing.

A diagnostic and prognostic technology for dedicated, real-time sensor analysis was studied by Roemer M. and Kacprzynski G. (2000). This work yielded performance anomaly detection and diagnosis with vibration fault detection in addition to component prognostics. This technology was developed for gas turbine engine health monitoring and prediction applications included an array of intelligent algorithms for assessing the total health of the engine, both mechanically and thermodynamically.

A model for diagnostics and prognosis of General Electrical gas turbines was developed by Frith and Karvounis (2001). Here models are presented: one estimated power assurance and the other detected abnormal engine operation. The first model for estimating power assurance call the T700 model-base was used with the Health Indicator Test (HIT) check. The HIT is checked with the power available for a given flight condition and scenario of component degradation. The second tool, a combined model

based detector and fuzzy-logic decision-maker is proposed initially for use in a Health and Usage Monitoring System (HUMS) ground station to reduce the amount of data manually processed or interrogated. The Defense Science & Technology Organization (DSTO) developed a MATLAB-Simulink true twin T700 engine model and demonstrated its accuracy in the tracking of transient flight data, (See figure 2.1).

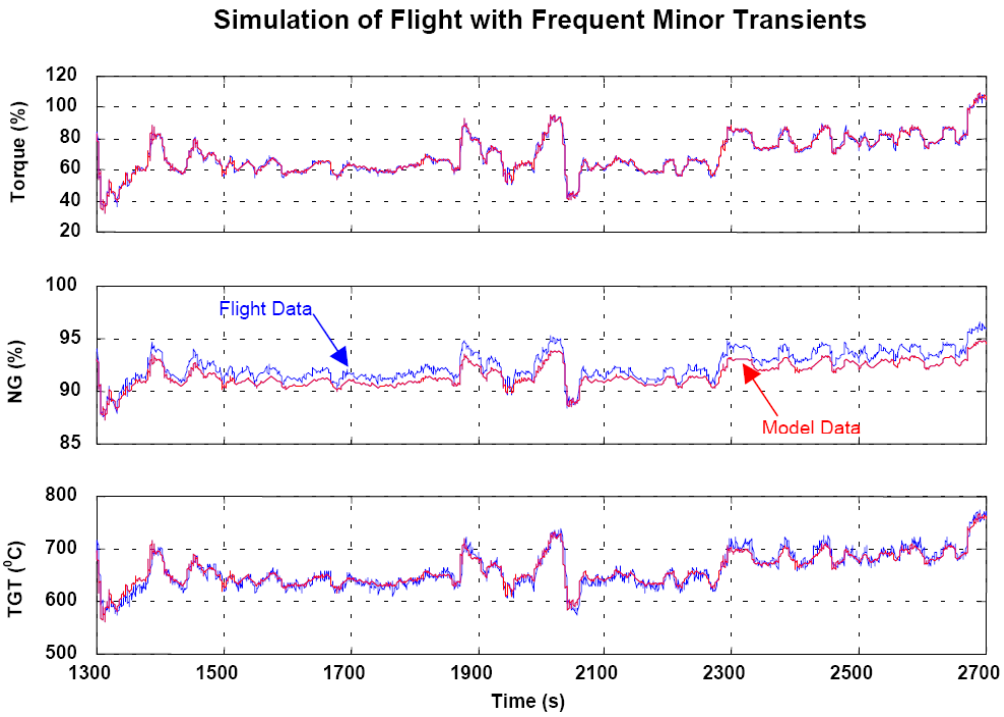

Figure 2-1: Tracking Capabilities of Simulink Model

A model based diagnostics method using a Neural Network and Genetic Algorithms was investigated by Kobayashi T. and Simon D. (2001). Neural networks were applied to estimate the engine internal health. Genetic Algorithms were used for sensor bias detection and estimation. This hybrid approach takes advantage of the nonlinear estimation capability provided by neural networks while improving the

robustness to measure uncertainty through the application of the Genetic Algorithms, (see Figure 2.2). The hybrid diagnostic technique also has the ability to rank multiple potential solutions for a given set of anomalous sensor measurements in order to reduce false alarms and missed detections.

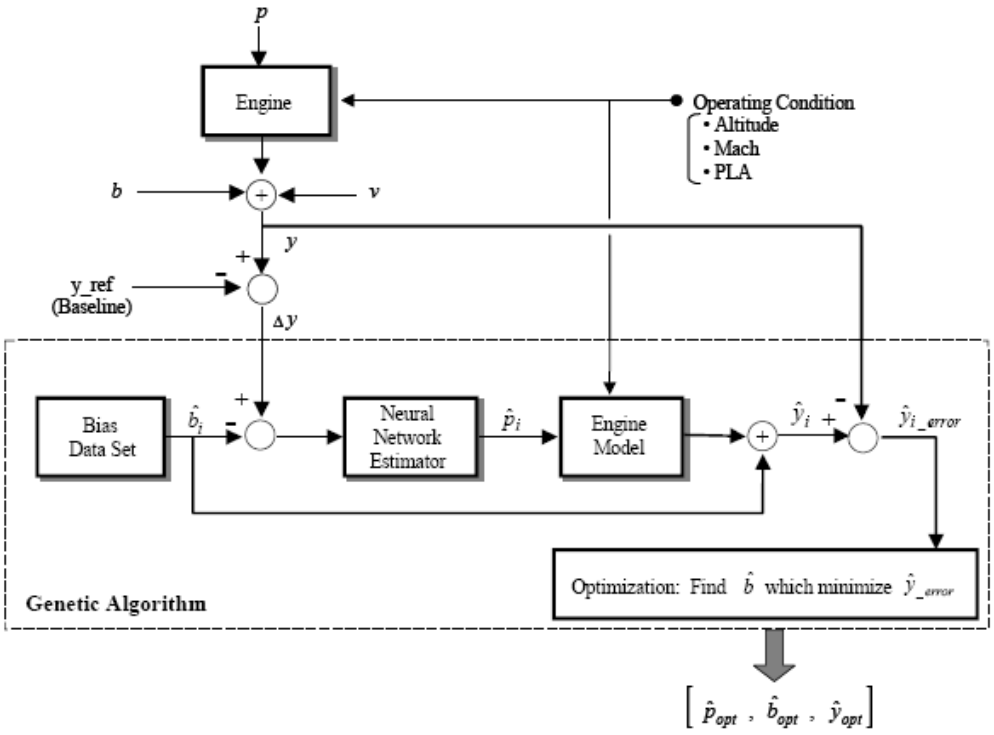

Figure 2-2: Genetic Algorithms architecture for the engine health

Here Aircraft engine performance diagnostics is accomplished by estimating a set of internal engine health parameters from available sensor measurements. These measurements, which include gas path temperatures and pressures, spool speeds, fuel flows, and variable geometry to name a few, provide information that can be used to determine the health of the engine. Engine performance deterioration is usually modeled by adjustments of efficiency and flow coefficient scalars of the following components:

Fan, Booster, High-Pressure Compressor, High-Pressure Turbine, and Low-Pressure Turbine. Genetic Algorithms (GA) were applied for sensor bias detection. The hybrid estimator exhibited excellent performance when at most one sensor was biased. The task of health parameter estimation became more difficult when the bias was of smaller magnitude and was thus less distinguishable from the standard noise level. Since measurement shifts due to health degradations are often small compared to sensor noise, and distinctive health degradations do not necessarily result in distinctive measurement shifts, thus it is difficult to obtain one solution with a high level of confidence. This problem was handled by ranking individuals in the GA population set based on their corresponding fitness values. The approach revealed a potential method of reducing the rate of false alarms and missed detections.

A feed forward neural network modeling the fuel flow to shaft speed relationship of a Roll Royse Spey aircraft turbine was used by Chiras N., Evans C. and Rees D. (2002). This model predicted the engine's performance, which helped develop a control system to predict normal engine behavior for on line fault detection purposes. Fuel flow and shaft dynamics is a nonlinear relationship. Here higher-order nonlinear thermodynamic models derived from the engine physics were reduced to linear models of the same order as the number of engine shafts. The models were first linearised at a series of operating points, using small perturbations, and then a model reduction procedure was employed. The identification problem in the time-domain for the linear modeling was to infer relationships between past input-output data and future outputs. A finite number of past inputs $u(t)$ and outputs $y(t)$ were collected into a vector $\varphi(t)$. A function f was developed that established a relationship between the next output

$y(t)$ and $\varphi(t)$, $\{y(t) \to f(\varphi(t))\}$. The function f can be any function, which defines the model structure. In the case for which f is a linear function several model structures are well documented such as ARX (Autoregressive with eXogenous inputs), ARMAX (AutoRegressive Moving Average with eXogenous inputs), (figure 2.4), OE (Output Error) and BJ (Box-Jenkins). ARMAX model structure was selected, because the structure was a recurrent network since the past prediction errors depend on the model output and consequently establish a feedback. The same applies to the OE and BJ networks. A mature body of work exists for the estimation of linear models in the time-domain.

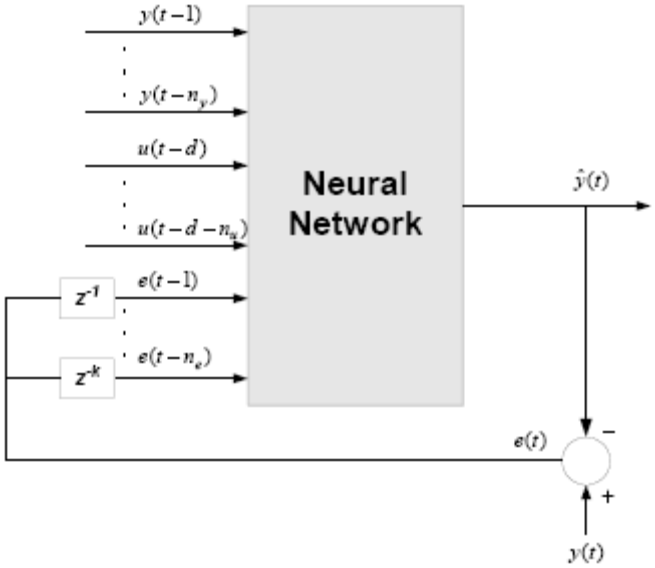

Figure 2-3: Neural Network ARMAX model structure

Sampath S. and Singh R. (2002) discussed diagnostics using Artificial Neural Networks (ANN), and Genetic Algorithm (GA). These techniques contributed to the management of available gas turbine used in industries. In this technique engine fault

diagnostics is treated as an optimization problem. The differences between observed data and synthetic data are minimized as an objective function of some model parameters. The synthetic data is generated using a known set of faults applied to the engine performance model and the minimum objective function is indicative of the problem. The application of genetic algorithm (GA) for the search of the global minimum, which represents the solution, was proven to be an efficient, flexible, robust and a reliable way of solving the engine diagnostics problems posed. Here GA based optimization techniques in gas turbine diagnostics showed to be very accurate even in the presence of a large amount of noise, bias and model inaccuracies.

In addition, Sampath S. and Singh R. (2002) presented results from Volponi (2001) that discussed a comparison between to Feed-Forward-Back Propagation Neural Networks and a Kalman Filter based model. Conventional technique likes Kalman Filters could be used to estimate the system's state and perform Strategy for Faults Diagnosis (SFDIA). The inherent limitations of these techniques suggest that a different approach could be pursued. The proposed advanced techniques represent a suitable tool for the SFDIA.

Gorinevsky D. and Nwadiogbu E. (2002), studied the diagnostics of a small turbine engine, a Honeywell 331-400 APU. Incipient fault estimation was performed from batch data by identifying deficiencies of the performance parameters in a detailed model of the engine. The algorithms include numerical estimation of the engine's acceleration from the noisy engine speed data (see figure 2.4), which was developed with a rigorously designed finite impulse response (FIR) differentiator. The FIR differentiator

had the following primary advantages: easy to implement, always stable, design methods is generally linear, can be designed to have linear phase. Which helps prevent distortion. The estimation approach is based on assuming that the performance parameters change is small and the respective system output change can be obtained through linearizing the model. The paper demonstrated that the location and magnitude of the performance faults could be estimated accurately despite the noise and nonlinearity, by using only exhaust gas temperature, compressor exit temperature, and engine speed data as prediction variables.

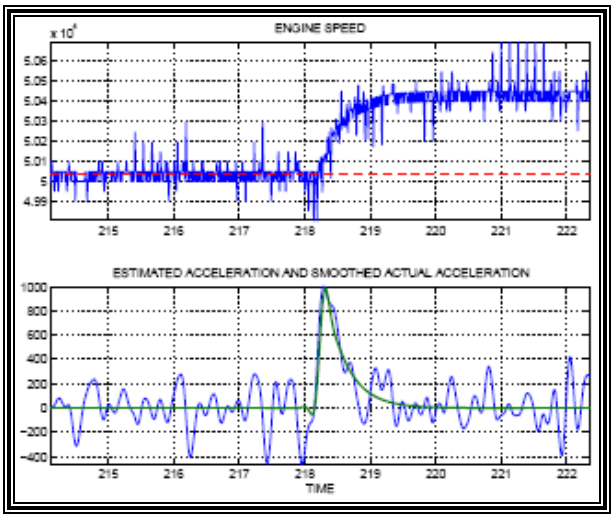

Figure 2-4: Estimation of engine acceleration from noisy engine speed data

Brotherton T. and Mahey R. (2001), investigated different types of anomaly detectors for the advanced military aircraft. Fusion of the anomaly detectors (ADs) with different approaches such neural networks (NNAD), physical models and hidden Markov models (HMM) reduced false alarms while at the same time improved detection performance. Table 1.1 shows a summary of the expected response for the different

detectors that were development. The types of anomalies are listed in the rows and the columns show expected response for each of the detectors. An 'X' indicates that the detector is expected to work while, a '?' indicates the response is not clearly known and depend on the data. In order to ensure that no anomaly class is missed, the method must have 'X's across each row. Two or more X's increased the probability of detections to reduce the false alarms.

Failure Type	**NNAD**	**BEAM**	**HMM**
Linear transform (gain)	**X**	**?**	**X**
Transient	**?**	**X**	**X**
New 'mode'	**X**	**?**	**X**
Feedback	**?**	**X**	**?**
Sensor failure (in range)	**X**	**X**	**?**
Sensor failure (noise)	**?**	**X**	**?**
Uncorrelated signals	**X**	**?**	**?**
Others	**?**	**?**	**?**

Table 2-1: Different anomaly detectors being development for the advanced military aircraft.

Link and Dong (2002), developed a hybrid model framework for anomaly detection with a health management system. A physics-based model receives on-line data as inputs and outputs estimated values for the variable of interest. The modeling approach is applicable to all the physical systems or subsystems of an aerospace vehicle. Using the modeling, anomaly detection is computed with the errors between the model estimate output and the variables values in anomaly test cases. An anomaly is determined by comparing the statistical tolerance band derived from nominal test cases. The model estimates obtained were better at steady states operation than in transient's events.

A new method to detect and compensate for a failure of one sensor in an array performing time delay based direction of arrival (DOA) estimation was presented by Pirinen T. (2004),. The detection was based on the planar wave assumption, which can be used to form confidence factors for time delays. Using these confidence factors we determine if one of the sensors in the array is producing improper data and has failed. After detection, all data from the failed sensor were discarded and DOA was computed without the data. The performance of the method was demonstrated with simulations, in which the proposed method was combined with typical time delay based DOA estimators.

Many engineering systems use sensors to monitor and control the operation of the system. In the case of gas turbine engines, these sensors are used to measure process variables such as rotor speeds, temperatures, pressures, and actuator position feedbacks. The sensor outputs are then used as feedback in a closed-loop operation to ensure that the system is being operated at the desired conditions and that safety bounds are being

observed, and that performance is being optimized.

Methods to detect, locate, and identify sensor degradations was investigated by Dorr R. and Kratz F. (1997). The first method is based on simple redundancy and consists in generating residuals by comparison of measurements provided by physically redundant sensors. The second uses analytical redundancy. The proposed analytical redundancy technique is based on steady-state relationships between measurements and could be applied to any process described by steady-state models. This approach was preferred to the dynamic approach since power plants operate mainly under steady-state conditions. Residuals are generated by comparing each measurement with an estimate computed from models of the process. The efficiency of each method is evaluated first on a simulated case and then on measurements obtained from a real power plant. In order to detect and locate the faulty sensors, drifts were simulated to test the efficiency of each method, and data reconciliation was used to estimate the magnitude of the faults and correct measurements. Faults are detected by comparing each residual with thresholds defined with respect to the sensor measurement accuracy. Degradation isolation consists in pinpointing the faulty sensors and requires an analysis of the relationships between residuals and measurements.

A robust fault diagnosis and validation strategy for temperature sensors and flow meters in central chilling plant was developed by Wang S. and Wang J. (2002), which is based on the first law of thermodynamics. The strategy evaluates soft sensor faults (biases) by examining and minimizing the sum of the squares of concerned mass or steady state energy balance residuals represented by the corrected measurement over a

period. It considers systematically all the concerned energy balances and obtains the best estimates of the sensor biases by minimizing the sum of the mean squares of normalized residuals of all energy balances involved. The genetic algorithm technique (GE) is employed to determine the global minimal solution to the multimodal objective function, which can be difficult to achieve by traditional gradient-directed search methods. Performance of an advanced robust fault detection, diagnosis and evaluation (FDD&E) scheme is compared with that of a sequential scheme, which was reported earlier, in simulation tests. The robust scheme is superior to the sequential scheme in determining abrupt sensor faults, such as biases. The robust scheme is applied to a central chilling plant in an existing commercial building, providing satisfied bias estimates. As a basic method, the sensor FDD&E strategy is of practical value in heating, ventilation and air-conditioning (HVAC) systems as well as in systems where the measurements of liquid low variables are essential in control and performance monitoring.

In addition, an effective method for sensor fault detection and identification (MSPCA) was developed by XU Tao and Wang Qi (2006). This method is known as multi-scale principal component analysis (MSPCA). By wavelet decomposition of each sensor's output, MSPCA integrates PCA with multi-scale wavelet analysis to discriminate the sensor's faulty characteristics. For the purpose of sensor fault detection and identification, the data in the window is decomposed with a wavelet transform to acquire the coarse-scale coefficients. A square predictor error (SPE) was employed to detect the sensor drifting error and a sensor validity index (SVI) for fault sensor identification. The applicability and the effectiveness of this method were illustrated with an industrial boiler monitoring system sensor. The output of the sensors (pressure, steam

flow, feed-water flow) and establish the MSPCA with this correlative signal were implemented in sensor fault diagnosis to ensure the normal operation of the system.

A model based procedure analytical redundancy for the detection and isolation of faults in input-output control sensors of a dynamic system was investigated by Simani, Fantuzzi, and Beghelli (2000). The diagnosis system was based on state estimators, namely dynamic observers or Kalman filters designed in a deterministic and stochastic environment that uses residual analysis and statistical tests for fault detection and isolation. The state estimators are obtained from input-output data process and standard identification techniques based on ARX or errors in variables models, depending on the signal to noise ratio. The Kalman filter parameters, the model parameters and input-output noise variances, are obtained by processing the noisy data according to the Frisch scheme rules. The proposed fault detection and isolation tool has been tested on a single-shaft industrial gas turbine model. Results from simulation show that minimum detectable faults are perfectly compatible with the industrial target of this application.

3 Principle and Background

3.1 Dynamic Response of Temperature Sensors

Gas turbines parameters are measured by zero, first and even second-order sensors during operation. Thermocouples are usually located in the engine compartment along various gas paths to measure flow temperatures. These devices are usually contained in a protective sheath and consist of a thermo-junction formed by welding, soldering, or merely pressing two wires of two different materials together. Consider a typical thermocouple placed along a gas flow path receiving heat from the surrounding fluid has shown in Figure 3-1 below:

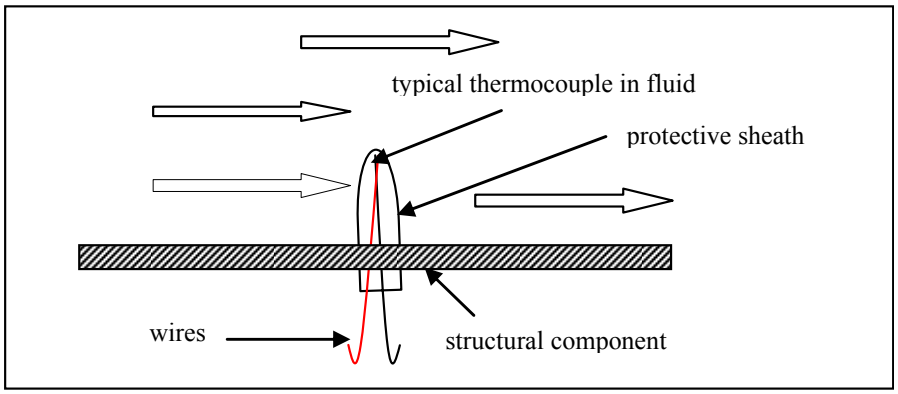

Figure 3-1: Typical thermocouple placed along a gas flow path

The time constant is a parameter that can be used in describing the dynamic response of an instrument and is an important consideration when choosing thermocouples sensors, Ogata, K. (1992). The time constant is a measure of the speed of response of an instrument to changing input conditions. Instruments with short time

constants are needed for measuring rapidly fluctuating phenomena, such as the velocity of a turbulent flow; whereas instruments with long time constants, such as the alcohol-in-glass thermometer, are used primarily for static measurements.

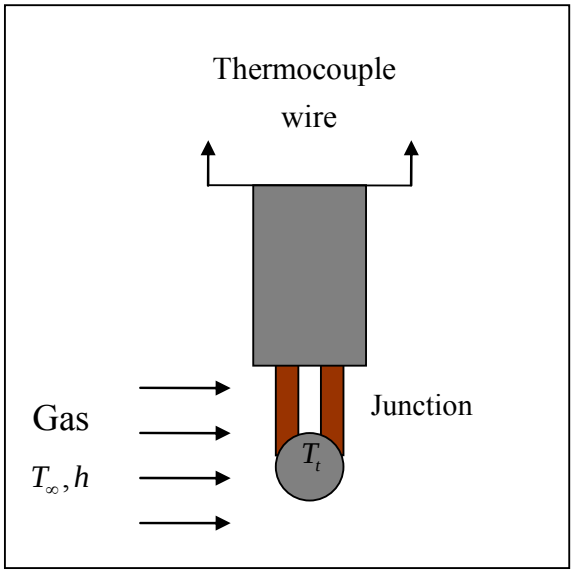

Figure 3-2 Thermocouple scheme

Let's consider the following analysis of the thermocouple depicted in Figure 3-2, to better understand the origin of the time constant. The temperature indicated by the thermocouple T_t, is the instantaneous temperature of the sensing element. If the temperature of the surroundings, T_∞, is different from T_t, heat transfer, Q, between the thermocouple and the surroundings can be expressed as:

$$Q = hA(T_\infty - T_t) \qquad 3\text{-}1$$

Where A is the surface area of the sensing element (in this case the bulb), and h is the convective heat transfer coefficient due to the motion of air surrounding the

thermocouple. As a consequence of the heat transfer, the thermocouple temperature will increase at a rate $\frac{dT_t}{dt}$ in which Q can be expressed as:

$$Q = mc\frac{dT_t}{dt} \qquad 3\text{-}2$$

In equation (3.2), m is the mass of the bulb of the thermocouple, c is specific heat, and t is time. Combining equations (3.1) and (3.2), yields the mathematical model of the thermocouple system as:

$$\left[\frac{mc}{hA}\right]\frac{dT_t(t)}{dt} + T_t(t) = T_\infty \qquad 3\text{-}3$$

When the first-order heat transfer equation is expressed in the form given by Equation 3-3 . The quantity [mc/hA] is called the time constant of the system. The time constant is usually refered to by, τ , and is express as:

$$\tau = \frac{\rho Vc}{hA} \qquad 3\text{-}4$$

Here the mass, m , has been substituted by the equivalent density volume relationship, ρV .

Where ρ , is the density of the sensor and V is the volume of the sensor. Equation (3.3) is a first order differential equation. Instruments that behave according to this type of equation are called first-order systems and sensors with this characteristic are called First-order sensors.

3.2 Resistance-Capacitance (RC) Circuit Model

Consider the resistance-capacitance (RC) circuit shown in Figure 3.3.

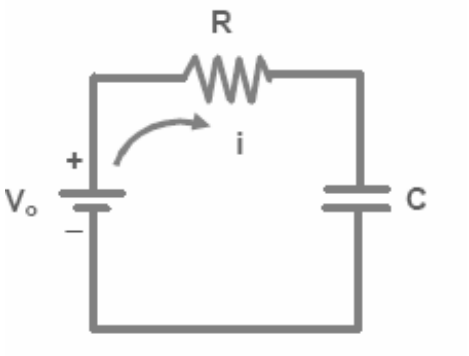

Figure 3-3: RC Electric Circuit Model

The circuit consists of a resistor of value, R, and capacitor of capacitance, c, in series with an applied voltage, V_0, that is generated with variable source. The voltage across the capacitor will be refered to has V_C and that across the resistor will be V_R. Application of Kirchhoff's voltage law yields:

$$-V_0 - Ri + \frac{1}{C}\int idt = 0 \qquad 3\text{-}5$$

here i is the current flowing in the circuit.

The voltage relationship across a capacitor is given by $V_C = \frac{1}{C}\int idt$. Solving for the current i and substituting this result in terms of voltage V_C, can change equation 3-5 to:

$$(RC)\frac{dV_c}{dt} + V_c = V_s \qquad 3\text{-}6$$

Note that equation 3.6 is of the same form as equation 3.3. Similarly, the product (RC) is the time constant, τ , of the circuit. Here R is the resistance measured in ohms, and C is capacitance measured in Farads (1 μfd = 10^{-6} Farad). The time constant, τ , is has units of seconds.

3.3 Analogy between thermal and electrical RC measurement system

The previous sections we studied two first-order systems, a thermal and electrical (RC) system. This section presents the analogy between both systems.

	RC CIRCUIT	**THERMOMETER**
τ **(Theoretical)**	**RC**	$\frac{mc}{hA}$
X **(Measured quantity)**	V_c **: Voltage across capacitor**	T_t **: Temperature indicated by thermometer**
X_s **(Forcing quantity)**	V_s **:Voltage across signal generator**	T_∞ **:Temperature of surrounding**

Table 3-1: Analogy between thermal and electrical RC circuit system

The general governing equation of the thermal and electrical systems described is of the form:

$$\tau \frac{dX}{dt} + X = X_s \qquad 3\text{-}7$$

Where:

X_s represents time-varying quantity we are measuring

X is time-varying output from our measurement system (this is the observed quantity).

τ This is the time constant of our measurement system.

It is interesting to know that the time constant depends upon the physical properties of the system and is independent of the measured quantity. A measurement system with a small time constant will respond quicker to changes than a system with a large time constant.

3.3.1 Step Response of First Order Thermocouple Sensor

This section will describe the response of a first order system to a step input. Consider the step input shown in Figure 3-4 described by:

$$X = 0 \quad ; \quad t \le 0$$
$$X = X_0 \; ; \quad t \ge 0$$

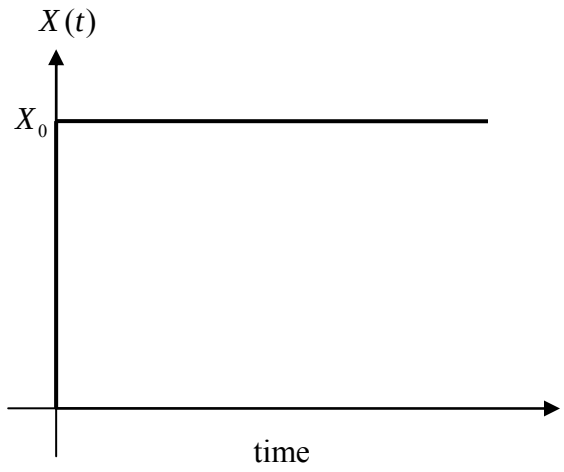

Figure 3-4: Step Input

To obtain the step response of the first order measurement system, first take the Laplace transform of equation (3.7).

$$L\left(\tau\frac{dX}{dt}+X\right)=L\left(X_s(t)\right) \qquad 3\text{-}8$$

Hence

$$\tau[sX(s)-X(0)]+X(s)=X_s(s) \qquad 3\text{-}9$$

Where $X(s)$ and $X_s(s)$ are the Laplace transform of $X(t)$ and $X_s(t)$ respectively, and $X(0)$ is the initial condition, which will be taken has zero. By solving for $X(s)$ equation 3.9 yield the transfer function of the system given by:

$$\frac{X(s)}{X_s(s)}=\frac{1}{\tau s+1} \qquad 3\text{-}10$$

Considering the step input function as $X_s = X_o$ = constant for $t \geq 0$ and substituting in equation (3.10), yields the output of the system as:

$$X(s) = \frac{1}{\tau s + 1}\left[\frac{X_0}{s}\right] \qquad 3\text{-}11$$

The inverse Laplace transform of this equation can be given by:

$$X(s) = X_0(1 - e^{-t/\tau}) \qquad 3\text{-}12$$

The Figure 3-4 depicts response of the system for three different first order systems with different time constants.

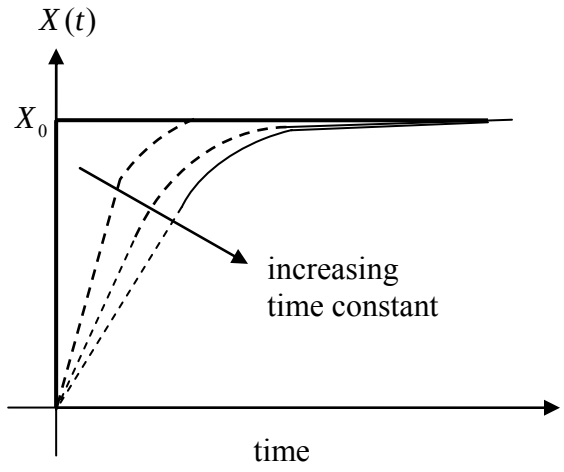

Figure 3-5: Step Response of first order system

By examining Figure 3-4 several things may be observed:

1. Even though the output starts to change immediately, a first order system can never respond instantly to an input.
2. The smaller the time constant, the quicker the system responds. The large time

constants lead to slow response.

3. For a step input, the output is asymptotic and never quite reaches the input.

4. There is never an overshoot the output is always smaller than the input.

3.3.2 Ramp Response of First Order Thermocouple Sensor

This section will be describing the response of the first order system to a ramp input. Consider the ramp input shown in Figure 3-6 described by:

$$X = X_i = 0 \; ; \quad t \le 0$$
$$X = At \quad ; \quad t \ge 0$$

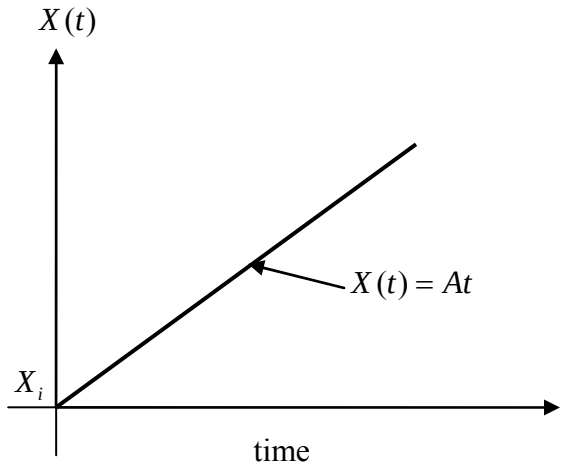

Figure 3-6: Ramp Input Function

To obtain the step response of the first order system, first take the Laplace transform of equation (3-7).

$$L\left(\tau \frac{dX}{dt} + X\right) = L\left(X_s(t)\right) \qquad 3\text{-}13$$

Hence

$$\tau[sX(s) - X(0)] + X(s) = X_s(s) \qquad 3\text{-}14$$

Where $X(s)$ and $X_s(s)$ are the Laplace transform of $X(t)$ and $X_s(t)$ respectively, and $X(0)$ is the initial condition, which is also $X(0) = 0$. By solving for $X(s)$ equation 3.14 yield the transfer function of the system given by:

$$\frac{X(s)}{X_s(s)} = \frac{1}{\tau s + 1} \qquad 3\text{-}15$$

Considering a ramp input function such as $X_s(t) = At$ for $t \geq 0$. Substituting in the equation (3-15), yields the output of the system as:

$$X(s) = \frac{1}{\tau s + 1}\left[\frac{A}{s^2}\right] = A\left[\frac{1}{s^2} - \frac{\tau}{s} + \frac{\tau}{\tau s + 1}\right] \qquad 3\text{-}16$$

The inverse Laplace transform of this equation can be given by:

$$X(t) = A(t - \tau + \tau e^{-t/\tau}) \qquad t \geq 0 \qquad 3\text{-}17$$

Figure 3-7 depicts a graph for two different first order systems responding to the ramp input with different time constants.

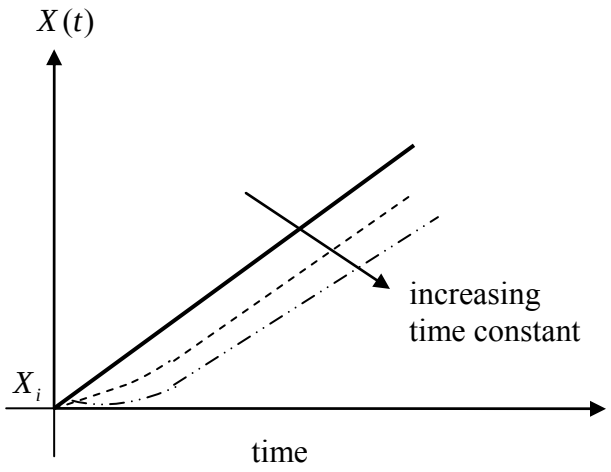

Figure 3-7: Ramp Response of First Order System

By examining Figure 3-7 the following can be observed:

1. The output does not immediately start to respond to the input (zero slope at t = 0).
2. The larger the time constant, the more the output lags behind the input.
3. The output is always smaller than the input.

The transient of a first order system usually takes 4 values of the time constant to reach 98% of the measured value. For $t \geq 4\tau$, the response remains within 2% of the final value. In practice, a reasonable estimate of the response time is the length of time that the response curve needs to reach the 2% line of the final value or four time constants. This transient region should be very short in duration compared to the varying signal. When a ramp has been applied for a long time, (greater than 4τ), the output becomes a straight line, parallel to the input. By letting the time be considerably large, it is possible to estimate the time measurement error.

Mathematically, we can solve the output equation for large t with:

$$e(t) = At - X(t) = A\tau(1 - e^{-t/\tau}) \qquad 3\text{-}18$$

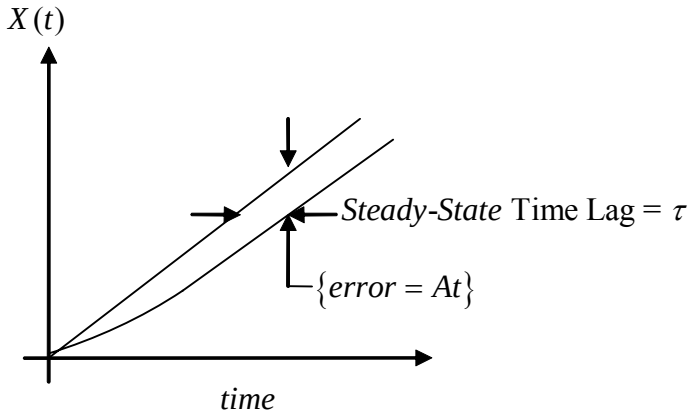

Figure 3-8: Ramp response of first order instrument

The error between the ramp input At and the response $X(t)$ is show in Figure 3-8. The error in the ramp input is equal to At for a large time, t. The smaller time constant, τ, the smaller the steady state error.

3.4 Background and Physical Errors in Temperature Sensors

A thermocouple is a temperature sensor that consists of two dissimilar metals joined together at one end (a junction) that produces a small thermoelectric voltage when the junction is heated. Thermocouples are available in different combinations of metals. The four most common configurations are: J, K, T and E. Each configuration has a different temperature range and environment. Another way to classify a thermocouple is

by the junction style as shown in Figure 3-9.

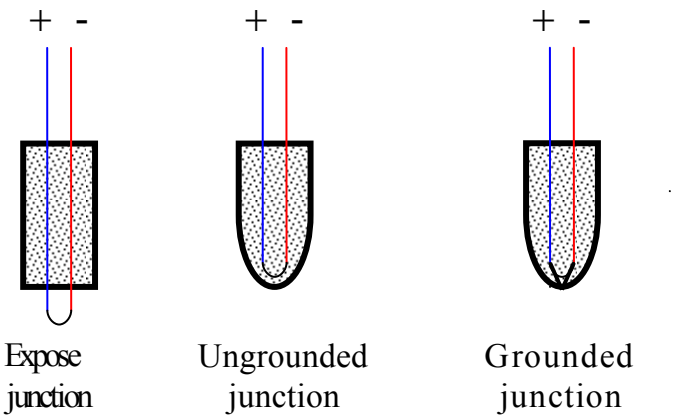

Figure 3-9: Three junction types of thermocouples

Thermocouples with expose junctions are generally used to measure gas temperatures in which extremely fast response times are required. The junction extends beyond the protective sheath to give accurate fast response. The sheath insulation is sealed where the junction extends to prevent penetrations of moisture or gas which could cause errors. The thermocouple probe with an ungrounded junction is recommended for measurements in corrosive environments where it is desirable to have the thermocouple electronically isolated from the protective sheath. This is particularly advantageous when measuring in areas where electric noise is present. The sheath may be electrically grounded, to provide a low impedance path for electrical noise to travel, keeping the measurements stable and accurate. The grounded probe combines advantages of excellent response time with the protection of a sealed sheath. It is recommended for the measurements of static or flowing corrosive gases and for high pressure applications.

4 Development of an Anomaly Detection Model for Temperature Sensor

4.1 Virtual Model of Temperature Sensors

Well designed thermocouples usually consist of long fine wires with axial and heat conduction reduced to a minimum. In analysis it is usually assumed that both the conductive and radiation heat transfer are negligible when compare to the convective heat transfer, Hung, Irwin and Kee (2004). Consider a thermocouple being heated in a bath of constant temperature T_∞ as depicted in Figure 4-1. The thermocouple has the following properties, a mass of m, and specific heat of c_p with an expose area, A, having a convective heat transfer coefficient, h.

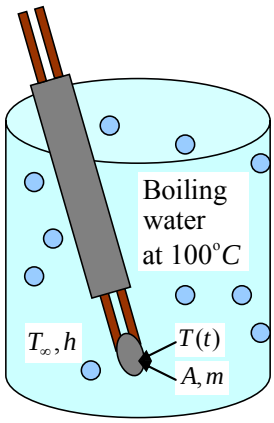

Figure 4-1: Thermocouple being heated in a bath of constant temperature T_∞.

By performing an energy balance and assuming that energy is transferred primarily by convection, the following equation may be derived.

$$\left[\frac{mc}{hA}\right]\frac{dT_t(t)}{dt}+T_t(t)=T_\infty \qquad 4\text{-}1$$

Equation 4.1 represents a simplified thermocouple model that has the general form of first order differential equation given by:

$$\tau\dot{T}+T=f(t) \qquad 4\text{-}2$$

Where ($\dot{T}$) is the time rate of change of the output sensor, τ is a time constant, $f(t)$ is the forcing function (input signal), and T is the output sensor. Solving for the first derivative yields

$$\dot{T}=\frac{1}{\tau}[f(t)-T] \qquad 4\text{-}3$$

Equation 4-3 can be solved analytically or numerically depending upon the function $f(t)$. A numerical solution using Simulink, a graphical interface for solving differential equations, was used to solve equation 4-3 as depicted in Figure 4-2.

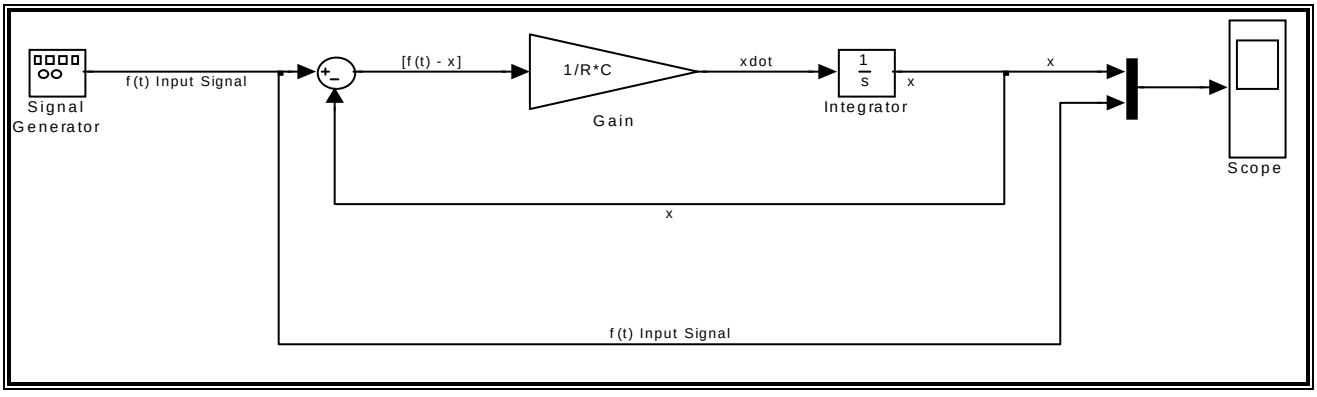

Figure 4-2: Virtual Model of Temperature Sensor

Figure 4-2 represents a Virtual Model of Temperature sensor as described by equation 4-2.

4.2 Time Constant Identification Algorithm

In order to develop algorithm to determine changes in the time constants of thermocouples, (detecting faults), consider the first order system described by equation 4-4 with input $u(t)$ and initial condition T_o.

$$\tau \frac{dT}{dt} + T = u(t)$$
$$T(0) = T_0 \qquad 4\text{-}4$$

Equation 4-4 may be transformed into equation 4-5 by taking the Laplace transform.

$$kST(s) - T(0) + T(s) = U(s) \qquad 4\text{-}5$$

Here T(s) and U(s) represents the Laplace transform of T(t) and u(t) respectively and T(0) is the initial condition, T_o.

By rearranging terms, equation 4-5 may be rewritten into the following form given by equation 4-6.

$$\frac{T(s)}{U(s) + T_0} = \frac{1}{\tau s + 1} \qquad 4\text{-}6$$

Considering a step function of the form:

$$u(t) = a \text{ for } t \geq 0$$

and substituting into equation 4-6 yields an expression for the temperature of the thermocouple.

$$T(s) = \frac{1}{\tau s + 1}\left[\frac{a}{s} + T_0\right] = \frac{a}{s}\left[\frac{\tau}{\tau s + 1}\right] + \frac{T_0}{\tau s + 1} \qquad 4\text{-}7$$

Transforming equation 4-7 into the time domain yields

$$T(t) = a - ae^{-t/\tau} + T_0 e^{-t/\tau} \qquad 4\text{-}8$$

and taking the derivative of equation 4-8 yields

$$C(t) = \frac{dT}{dt} = \frac{a}{\tau}e^{-t/\tau} - \frac{T_0}{\tau}e^{-t/\tau} \qquad 4\text{-}9$$

An expression for the time constant may be obtained by examining the ratio of the time derivative at two instances t and $t + \Delta t$ as expressed as:

$$\frac{C(t)}{C(t+\Delta t)} = \frac{\left.\frac{dT}{dt}\right|_t}{\left.\frac{dT}{dt}\right|_{t+\Delta t}} = \frac{\frac{a}{\tau}e^{-t/\tau} - \frac{T_0}{\tau}e^{-t/\tau}}{\frac{a}{\tau}e^{-t+\Delta t/\tau} - \frac{T_0}{\tau}e^{-t+\Delta t/\tau}} \qquad 4\text{-}10$$

and may be rearranged to have the form of

$$\frac{C(t)}{C(t+\Delta t)} = \frac{e^{-t/\tau}}{e^{-t+\Delta t/\tau}} \cdot \frac{\frac{a}{\tau} - \frac{T_0}{\tau}}{\frac{a}{\tau} - \frac{T_0}{\tau}} = e^{\Delta t/\tau} \qquad 4\text{-}11$$

By taking the natural log of equation 4-11, an expression for the time constant can be obtained as:

$$\tau = \frac{\Delta t}{\ln\left(\frac{C(t)}{C(t+\Delta t)}\right)} \qquad 4\text{-}12$$

The equation 4-12 is valid only for a step function in which fluid temperature quickly varies and then remains constant for a given period of time.

By assuming that the time constant is fast, greater than 5 times its value for each time data is taken, the use of a ramp input,(At), to describe fluid temperature changes can be considered. Here the solution to equation 4-4 would yield the form of:

$$T(t) = At - A\tau u(t) + A\tau e^{-t/\tau} + T_0 e^{-t/\tau} \qquad 4\text{-}13$$

Were A is the slope of the input temperature given in degrees per unit time and τ retains its aforementioned definition. Taking the second derivative of the equation 4-13 yields

$$D(t) = \frac{d^2T}{dt^2} = \frac{A}{\tau}e^{-t/\tau} + \frac{T_0}{\tau^2}e^{-t/\tau} \qquad 4\text{-}14$$

again an expression for the time constant can be obtained by examining the ratio of the time derivative at two instantaneous t and $t + \Delta t$ as expressed by equation 4-15.

$$\frac{D(t)}{D(t+\Delta t)} = \frac{\left.\frac{d^2T}{dt^2}\right|_t}{\left.\frac{d^2T}{dt^2}\right|_{t+\Delta t}} = \frac{\frac{a}{\tau}e^{-t/\tau} + \frac{T_0}{\tau^2}e^{-t/\tau}}{\frac{a}{\tau}e^{-(t+\Delta t)/\tau} + \frac{T_0}{\tau^2}e^{-(t+\Delta t)/\tau}} \qquad 4\text{-}15$$

By rearranging terms we obtain

$$\frac{D(t)}{D(t+\Delta t)} = \frac{\left.\frac{d^2T}{dt^2}\right|_t}{\left.\frac{d^2T}{dt^2}\right|_{t+\Delta t}} = \left(\frac{e^{-t/\tau}}{e^{-(t+\Delta t)/\tau}}\right)\cdot\frac{\frac{a}{\tau}+\frac{T_0}{\tau^2}}{\frac{a}{\tau}-\frac{T_0}{\tau^2}} = e^{\Delta t/\tau} \qquad 4\text{-}16$$

Taking the natural log of equation 4-15, yields an expression of the form of equation 4-12 for the time constant can be obtained as:

$$\tau = \frac{\Delta t}{\ln\left(\frac{D(t)}{D(t+\Delta t)}\right)} \qquad 4\text{-}17$$

With the equation 4-17 it is possible to calculate on a time to time base the time constant of the first order sensor.

We are now in a position to develop an algorithm to determine the time constant. Assuming that the actual sensor output is produced by a continuous piece wise ramp input, discrete time derivatives may be taken to estimate the time constant using equation 4-17. It is expected that variations of the time constant will occur and by performing a histogram of the value calculated, a best estimate of the time constant of the system may be obtained. Summarized below are the steps used in the algorithm:

1. Filter the input signal
2. Calculate the first derivative
3. Filter the signal again
4. Apply the second derivative
5. Store time constant data in virtual memory (buffer) at the actual time new data is processed during the time window interval.

As an example consider the thermocouple data given in Figure 4-3. The time constant calculations were determined with the described algorithm and are show in the histogram in Figure 4-4. The thermocouple data is given in Appendix A-1

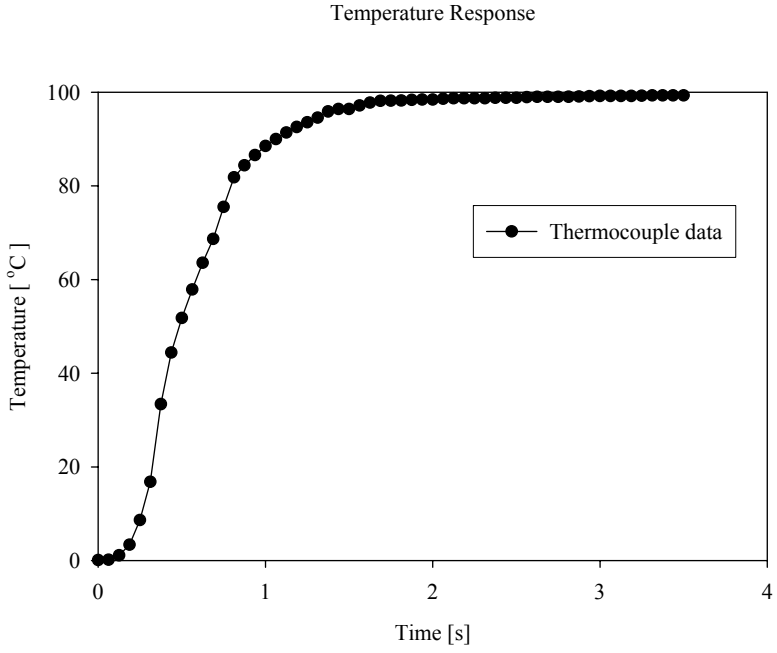

Figure 4-3: Thermocouple data

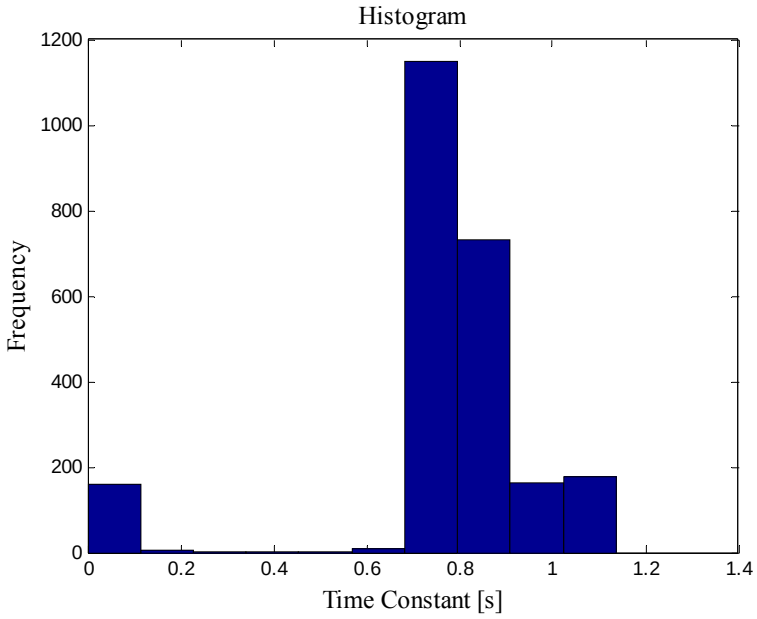

Figure 4-4: Time constant

By examining the histogram in Figure 4-4, it can be seen that the value with most frequency corresponds to 0.75 sec. Because the algorithm uses derivatives, its implementation presents some difficulties when the signal is contaminated with noise. However, by using filter techniques this situation can be overcomed.

4.3 Filters Implementation Using Experimental Data

Three types of filters were examined in this investigation. These correspond to the Moving Average Filter, the Exponential Average Filter, and the Exponential Average Smoothed Filter. In the example given in section 4-2 all the data taken in the experiment was used. Depending on the event being monitored, this procedure may not be practical and it may be more convenient to determine the time constant for a window of time that continuously accepts and eliminates new and old data respectively. This procedure is

depicted in the simulink-block diagram given in Figure 4-4. A brief descriptions of the filters used are given in appendix A-3.

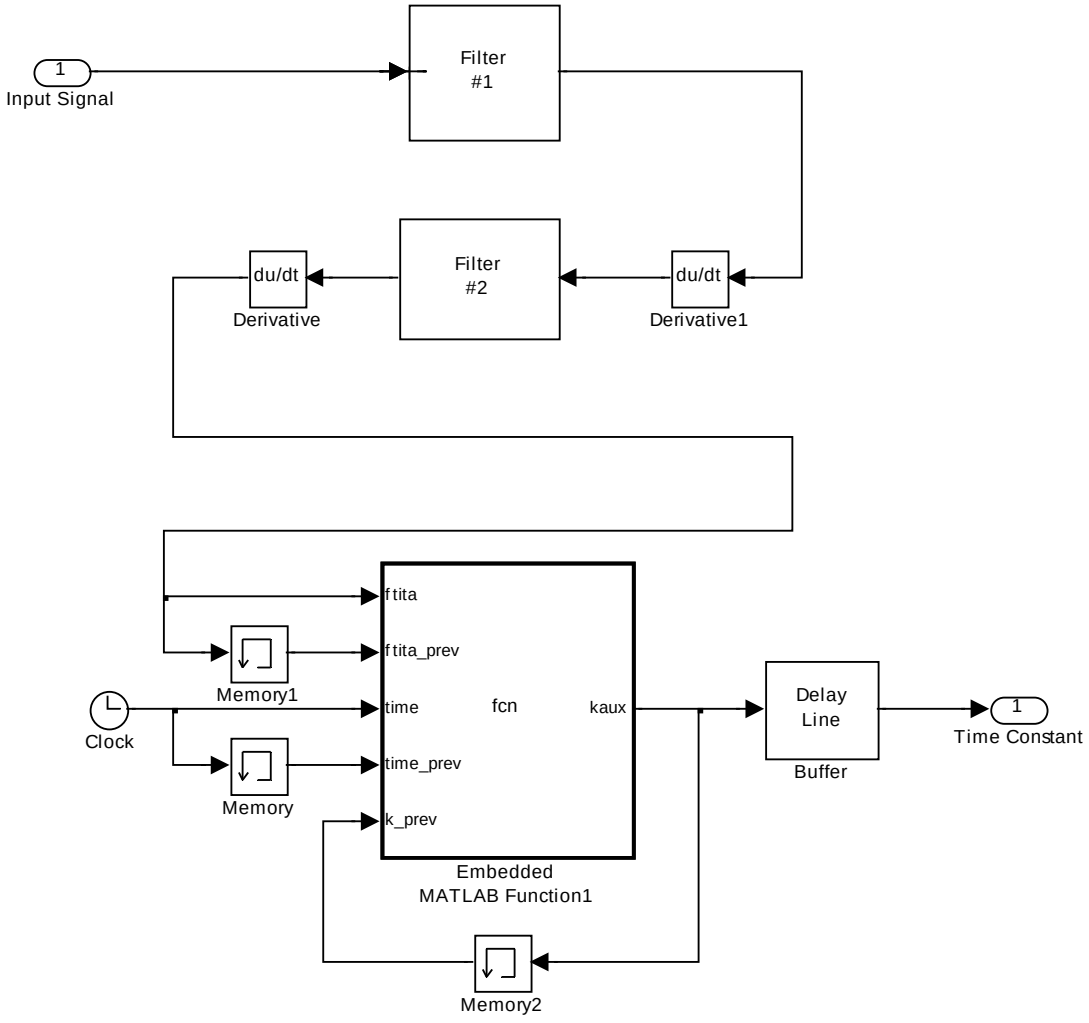

Figure 4-5: Anomaly detection algorithm for temperature sensors

By observing the algorithm in Figure 4-5, it can be seen that the filter is applied two times. First, on the temperature data, then on the derivative of that data. After words, is determined and the time constant is calculated. Here time constant data is stored in a virtual memory buffer at the same time new data is processed in the window interval.

It is important to note that in Figure 4-5, the buffer stores the previous information, but not all the information. This buffer is set with a capacity of storage. After that capacity is full, the oldest data is removed and this space is used to save the new or actual data. Then, the time constant is estimated with the data stored in the buffer. The value that is sent to the output, of the simulink block, is the mean value of all calculations with the available data at that time.

To examine how the filters works in this algorithm, different tests cases were studied. A particular temperature response was corrupted by random noise. Table 4-1 depicts the time constant variations with a noise corrupted thermocouple output using three different filters in the described algorithm.

Table 4-1: Time constant estimates with a noise corrupted thermocouple output using 3 filters

	Time Constant (sec)						
Noise Power	M.A.F.	% of ERROR	E.A.F.	% of ERROR	E. A. S. F.	% of ERROR	Temperature
{ZNOISE_VAR12}	Mean Value		Mean Value		Mean Value		% Signal Error
0	0.771	-	0.771	-	0.77	-	0
0.001	0.7717	0.09	0.7716	0.1	0.7704	0.05	7.65E-04
0.005	0.7726	0.21	0.7749	0.5	0.7783	1.08	0.0017
0.01	0.7732	0.29	0.7796	1.1	0.7856	2.03	0.0024
0.05	0.7761	0.66	0.8327	8.0	0.8573	11.34	0.0054
0.1	0.7785	0.97	0.8842	14.7	0.9073	17.83	0.0076
0.15	0.7807	1.26	0.8908	15.5	0.9334	21.22	0.0094
0.2	0.7825	1.49	0.9219	19.6	0.9176	19.17	0.0108

By examining Table 4-1 several things can be observed:

1. The original time constant is 0.771 sec.

2. The time constant changed by increasing the noise intensity in the signal.

3. Compared to the other Filters, the Moving Average Filter (M.A.F.) performed the best.

The prior results are represented in Figure 4-6.

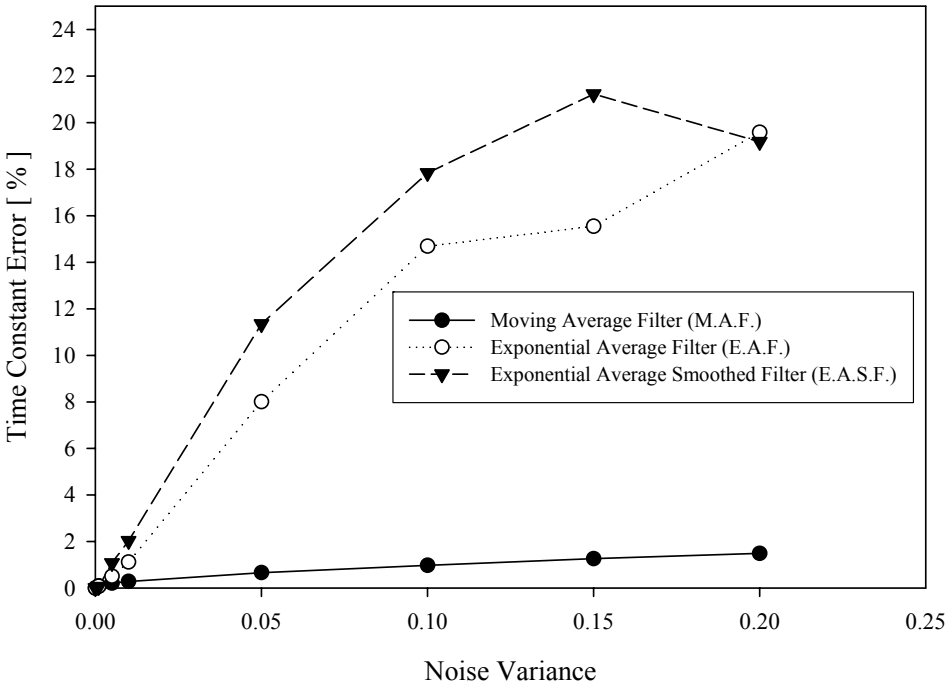

Figure 4-6: Time constant variation with a noise corrupted thermocouple output

To better understand how noise affected the time constant calculation, histograms using the various filters were compared with a noiseless reference signal for various levels of random noise as depicted in Figures 4-7, 4-8 and 4-9.

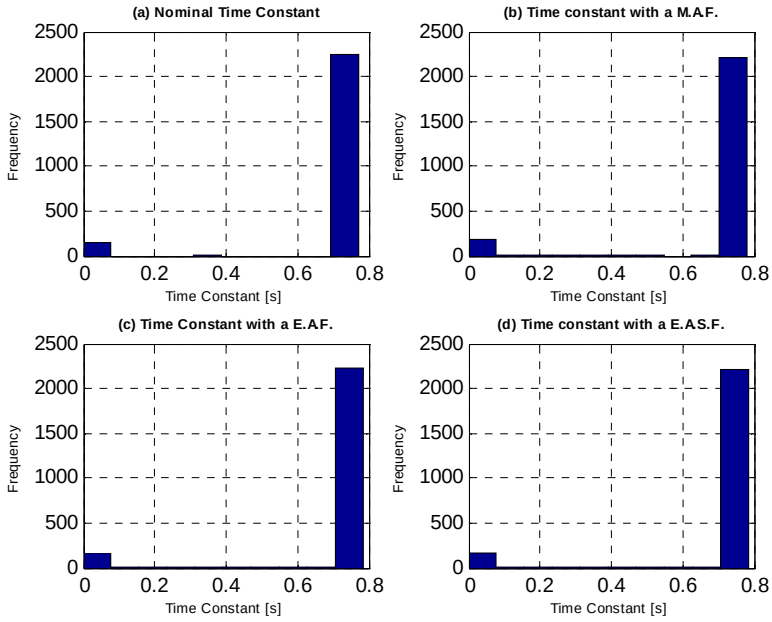

Figure 4-7: Time constant estimate with a noise variance = 0.001

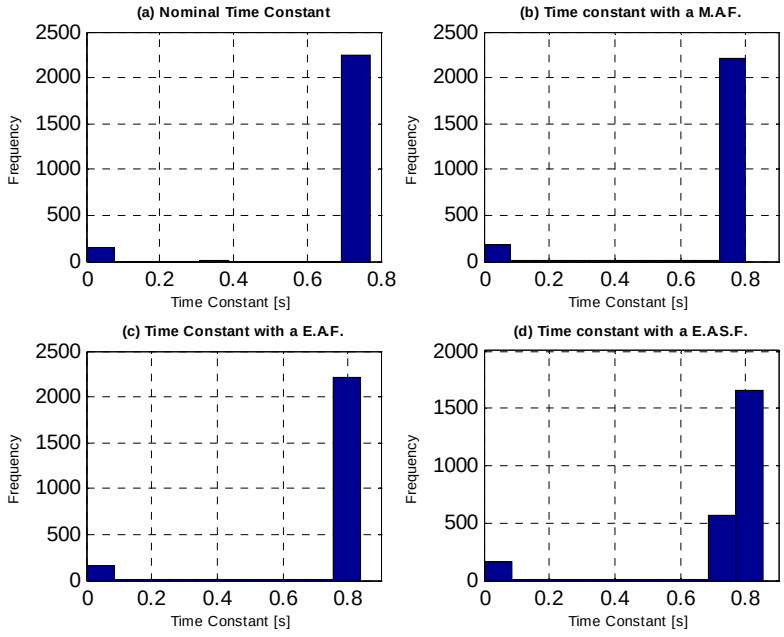

Figure 4-8: Time constant estimate with a noise variance = 0.01

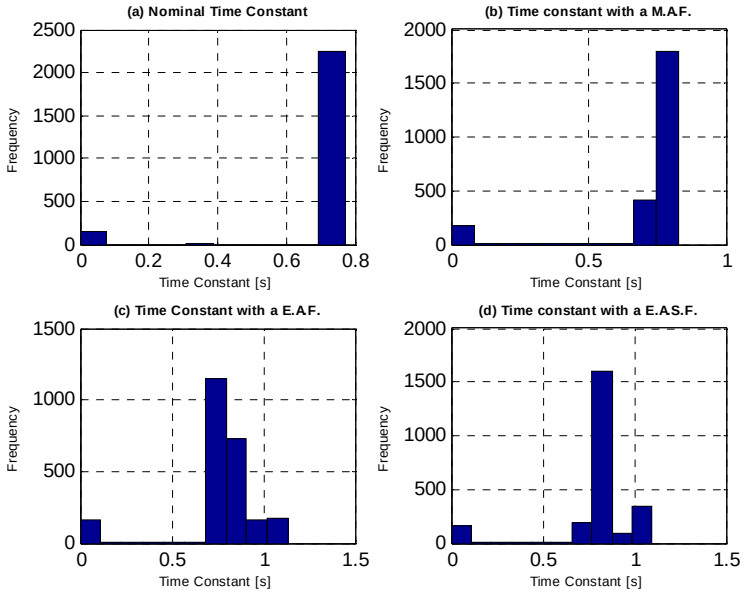

Figure 4-9: Time constant estimate with a noise variance = 0.05

By examining the priori figures, it can be appreciated that there is one value that appears more frequently than the others. These filters are sensitive when the signal is contaminated with noise. The Exponential Average Filter and Exponential Average Smoothed Filter were used from a Matlab tool box. These filters use one and two parameters respectively. The smoothing parameters must be values in the range [0.0 1.0]. The best value to use for the smoothing constants depends on the data being modeled.

When the signal was corrupted by noise, the moving average filter was the optimal solution for this problem. This filter provided the lowest error for a given temperature signal of a first order sensor. This moving average filter operates by averaging a number of points from the input signal to produce each point in the output signal.

5 Validation Model of Experimental Results

5.1 Experimental Study for Validation Model

To better understand the behavior of the thermocouple sensors, transient temperature reading were taken using two reservoirs at different temperatures. The experimental setup is depicted in Figure 5-1. Initially the thermocouple is immersed in an ice bath at a reference temperature of $0^{o}C$ and later moved to reservoirs of boiling water at $100^{0}C$. Transient temperature data was collected at a rate of 0.00125 sec per sample using a thermocouple data logger.

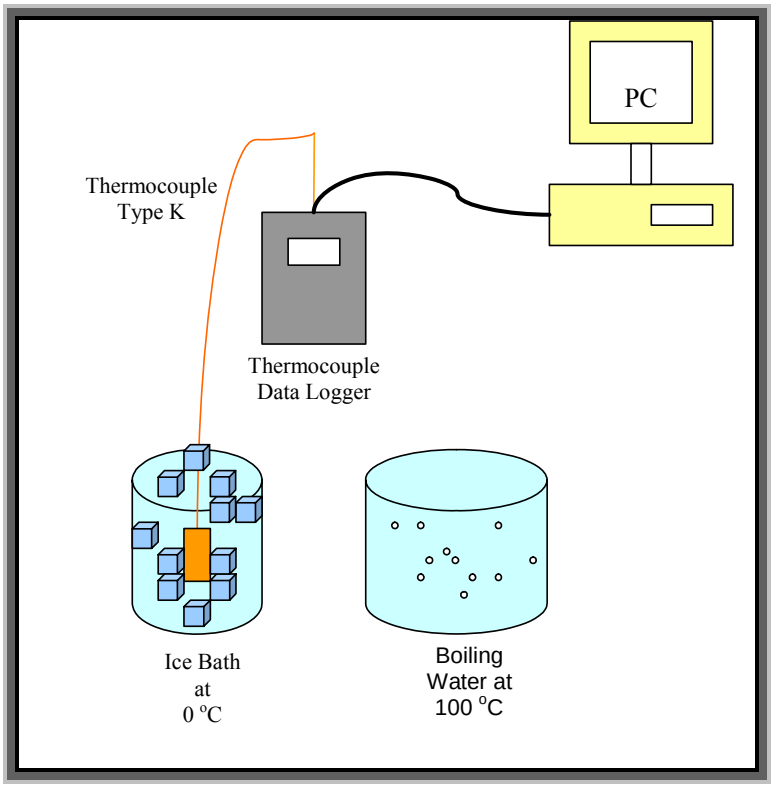

Figure 5-1: Experimental setup, two reservoirs at different sates $0^{0}C$ and $100^{o}C$ respectively

5.1.1 Case Study No. 1

The first phase of this experiment was to verify the effect of geometry on the time constant as predicted by chapter four. Four type K thermocouples using different construction configurations were examined. The first sensor, sensor #1, was constructed with a temperature bulb volume of 2.1 mm^2. The second sensor, sensor #2, was constructed with a temperature bulb volume of 1414.1 mm^2. The third sensor, sensor #3, was constructed with a temperature bulb volume of 1266.9 mm^2 and sensor #4 with a temperature bulb volume of 6710.0 mm^2. These sensors are depected in Table 5.1.

Sensor	Thermocouples Type K	Volume of bulb V_b(mm^3)
1	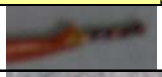	2.1
2		1414.1
3		1266.9
4		6710.0

Table 5-1: Thermocouples sensors with different volumes

Each thermocouple was immersed from the ice reservoirs to the reservoirs with 100^{o}C water. Figures 5-2 a, b, c and d shows the typical response of each sensor. Data was entered into the algorithm developed in chapter 4. The calculated time constants are given in Table 5-2.

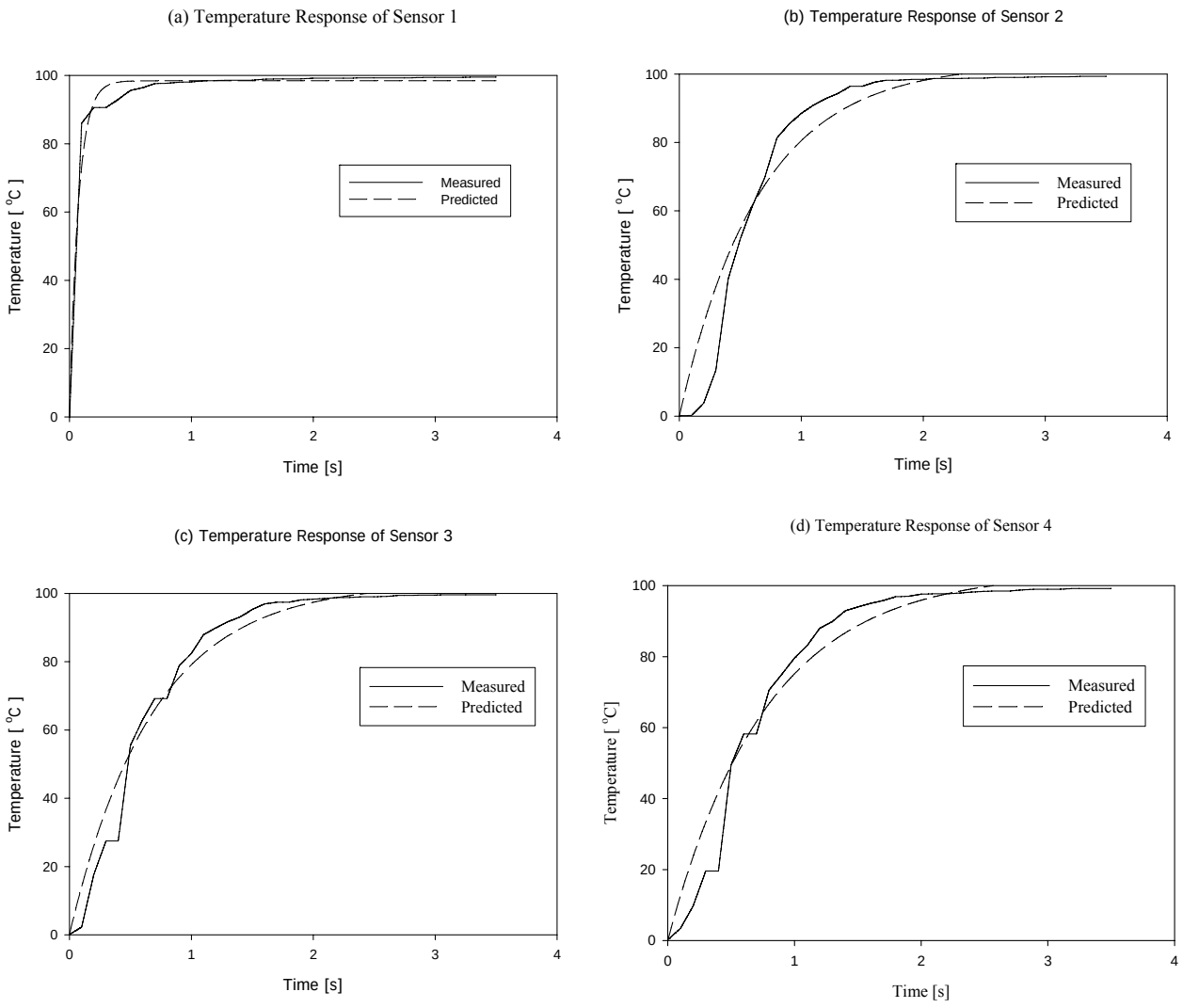

Figure 5-2: Thermocouple Sensors Responses changing the volume of a probe

Sensor	Time Constant (sec)
1	0.041
2	0.54
3	0.5
4	0.77

Table 5-2: Time constant of a sensors

It can be seen that as the volume increases, the time constant increases. By examining the definition, (mc_p / hA), of the time constant, this type of behavior is expected.

In order to investigate the feasibility of using transient data to determine thermocouple faults, damage was introduced into each thermocouple and the change in the time constant was observed. A summary of the various thermocouples used along with their corresponding conditions is given in Table 5-3.

#	Thermocouple Description	Normal Conditions	Damage Description
Sensor A-1	Represent typical welded thermocouple	Normal welded joint	N\A
Sensor A-2	Dissimilar wires material with a twisted joint	N\A	Twist joint
Sensor B-1	Represent typical welded thermocouple in contact well	Normal welded joint with contact well	N\A
Sensor B-2	Two dissimilar wires material with welded joint without well contact	N\A	Welded joint without well contact
Sensor B-3	Thermocouple painted in a surface probe	N\A	Painted probe (Black color)

Table 5-3: Normal sensors: A-1, B-1 “Damage” sensors: A-2, B-2, B-3

In addition to investigating the effects of changes in thermocouples probes, thermo junctions formed by welding were also studied. Here damage was simulated by twisting the thermocouple wires together. A typical response is given in Figure 5-3 along

with the time constant calculation shown in Table 5-4.

As seen from the table, sensor A-1 had initially a time constant of 0.041 sec when undamaged. After applying damage, sensor A-2, time constant varied 17.1 percent.

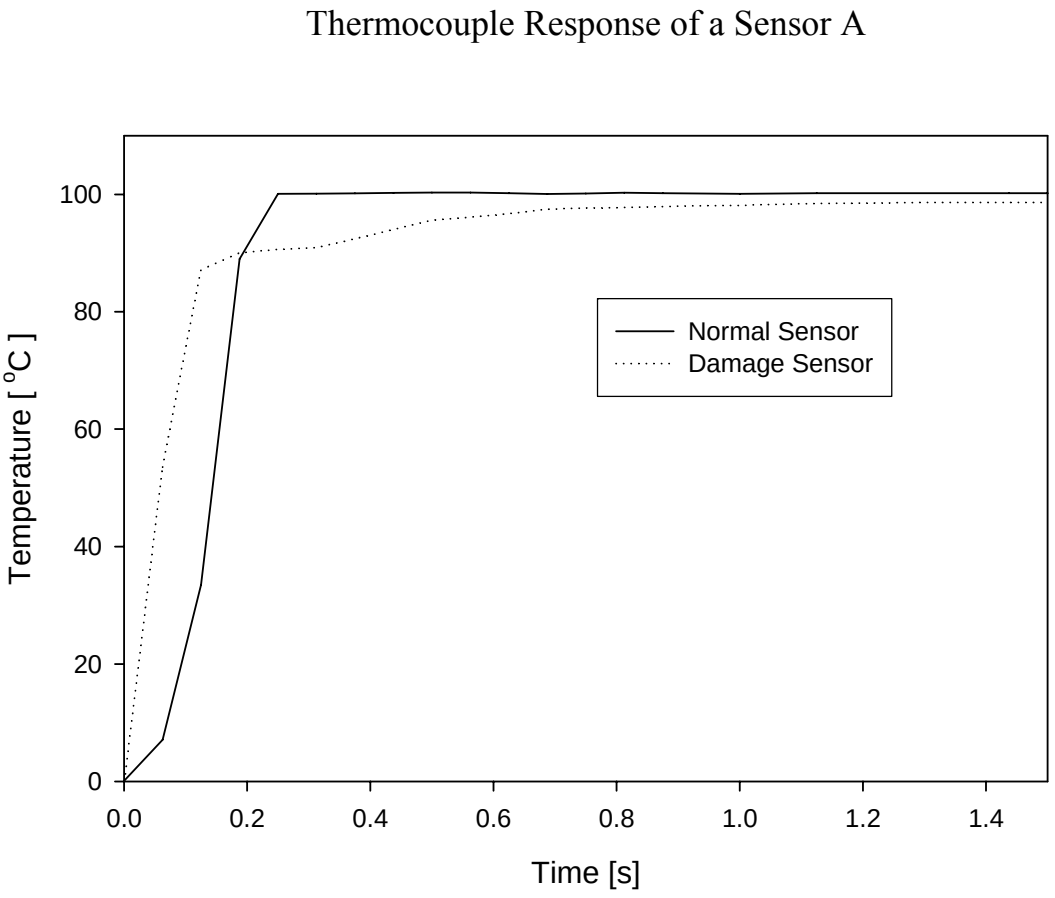

Figure 5-3: Thermocouple Sensors Responses with a Normal and a Damage conditions

Sensor	Condition	Time Constant (sec)
A-1	Normal	0.041
A-2	Damage	0.048

Table 5-4: Time constant calculation

By examining the Table 5-4 we can observe two different time constant calculation from the algorithm, a normal thermocouple and physical damage in a sensor. It's important to observe that the possibility to detect fails or anomalies in a temperature sensor using a time constant variation looks promising.

The effect of damage described in the various thermocouple sensors produced changes in the time constant as expected. The separation, lack of well contact or covering the surface with paint varied the heat transfer coefficient causing variations. Figure 5-4 and Table 5-5, shown the response and the time constant calculation using the algorithm respectively.

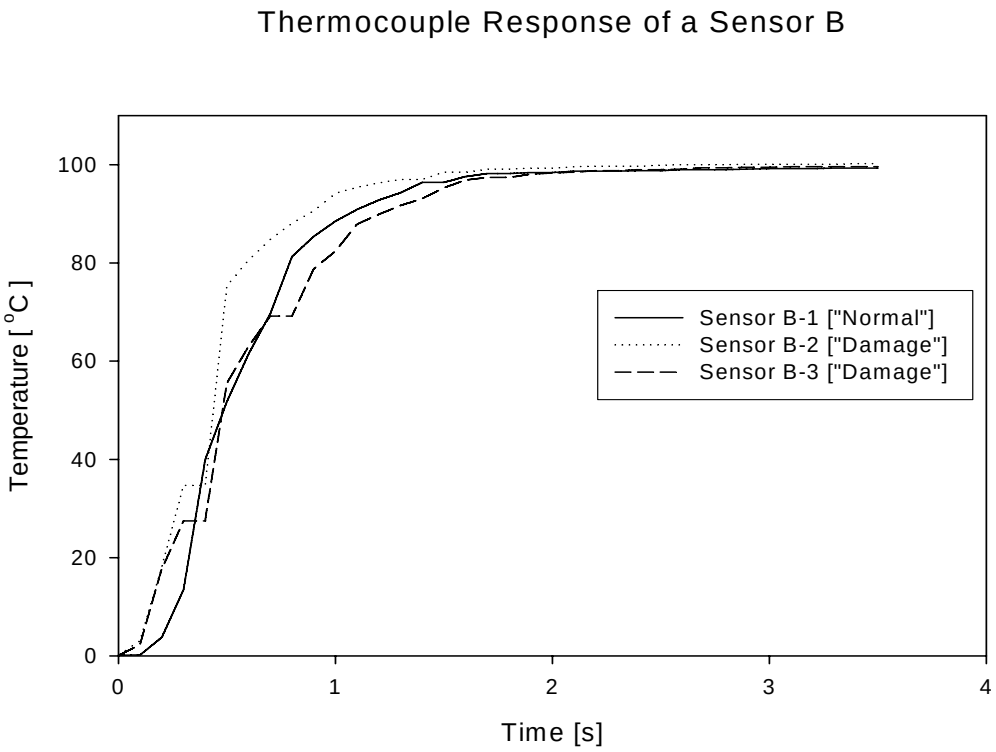

Figure 5-4: Thermocouples sensors responses with a normal case and two "damage" condition

Sensor	Condition	Time Constant (sec)
B-1	Normal	0.50
B-2	Damage	0.49
B-3	Damage	0.54

Table 5-5: Time constant calculations

As seen from the table, sensor B-1 had initially a time constant of 0.5 sec when undamaged. After applying damages in sensors B-2 and B-3, the time constant varied 2% and 8% respectively. As expected, has the value changes the time constant varies on so does the temperature response.

5.1.2 Case Study No. 2

In order to better simulate the conditions of temperature measurements in a gas turbine environment, air was heated through a copper tube of constant area as depicted in Figure 5-5.Here air enters at an ambient temperature of 85^{o}F using a fan running at a constant velocity with heat being added at constant rate into the system with a gas burner. The burner is shut off, when the system reaches a temperature of 405^{o}F. The temperature is measured in the exhaust section by a thermocouple device as shown in Figure 5-5. Transient thermocouple data is collected by a data logger instrument, and then feed into a computer through serial port as shown in Figure 5-5.

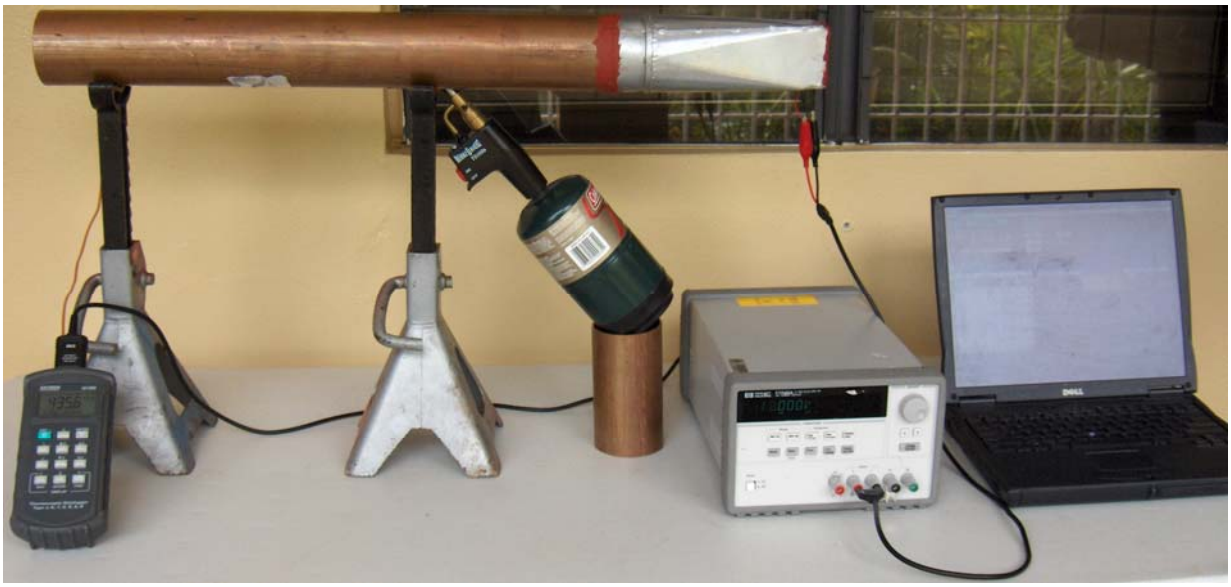

Figure 5-5: Experimental Setup Case 2

The speed of the response is a function of the time constant, $\tau = mc/hA$, that may be increased or decreased by varying the mass (m), specific heat (c), heat transfer coefficient (h) and the surface area (A). Some times the time constant can vary. When this occurs, it is generally due to changes in the heat transfer coefficient that depends on the surrounding fluid and its velocity. Figure 5-6 show the thermocouple response for two different velocities.

Instantaneous Exhaust Temperature Measurements
Using Thermocouple in Constant Velocity Flow Environments

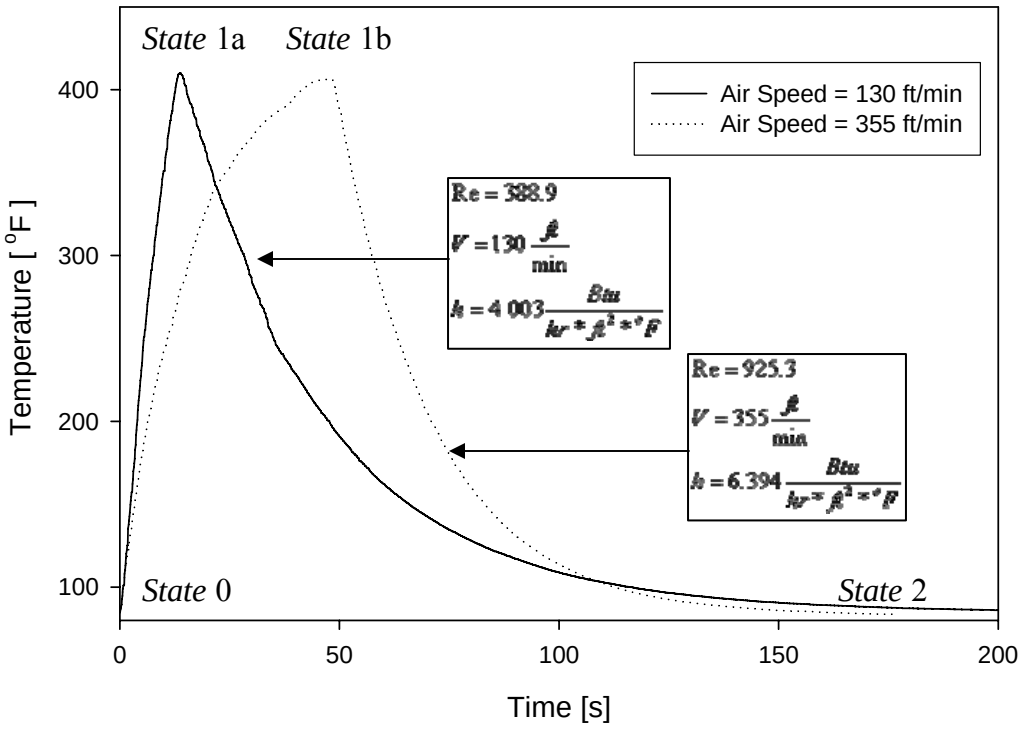

Figure 5-6: Exhaust Temperature Measure at Two Stream Velocity

Transient thermocouple data observed was collected and then the data was feed into a time constant identification algorithms. Table 5-6 presents the velocity effects in the time constant calculation of the thermocouple sensor estimated by the model.

No.	Air Speed (ft/min)	Time Constant (msec)
1	130	3.0
2	355	1.8

Table 5-6: Time constant of a sensor at two stream velocity

By examining the priori Figure 5-6, the thermocouple response labeled at a constant velocity of 355 fpm has a time constant of 1.8 sec. Note that once the thermocouples achieve the 405 °F temperature the one at the higher airflow in effect cools faster as expected. While heating up, the higher air speed affects the energy balance such that the convective losses increase and delay the energy storage (temperature increase). Therefore the thermocouple at the lower airspeed will heat up faster yet cool off slower. This is because heat transfer coefficient depends partly on the value of the film coefficient of heat transfer at the outside of the probe, which varies greatly with changes in fluid velocity. It's important to know that the heat transfer coefficient is in function of the velocity.

The behavior of this process can be modeled by Equations 5-1 and 5-2. These equations are obtain by performing and energy balance on the fluid in the tube and the thermocouple respectively.

$$\rho V_{air} A_{in} T_{air} - \left(hA_c\right) T_c + \dot{E}_{burner} = \rho_{air} c_p \forall \dot{T}_2 + \left(m_c c_{p_c}\right) \dot{T}_c \qquad 5\text{-}1$$

$$hA(T_{air,out} - T_c)] = m_c c_{p,air} \frac{dT_C}{dt} \qquad 5\text{-}2$$

Equations 5.1 and 5-2 represent the air heated through a copper tube and the simplified thermocouple model respectively. Where A is the surface area of the sensing element (in this case the bulb) and h is the convective heat transfer coefficient due to the motion of air surrounding, The air inlet and outlet temperature conditions are given by $T_{air,in}$ and $T_{air,out}$. T_c is the thermocouple temperature.

Two thermocouples sensors were used to measure the temperature in the exhaust section of the system show in a Figure 5-5. The normal thermocouple sensor consisted of a thermo junction formed by welding. Were as the damage sensors in this experimental study was created by bonding two dissimilar wires with a twisted joint. The response of each sensor is show in the Figure 5-7. The time constant for this sensors was calculated using the algorithm and is summarized in Table 5-7.

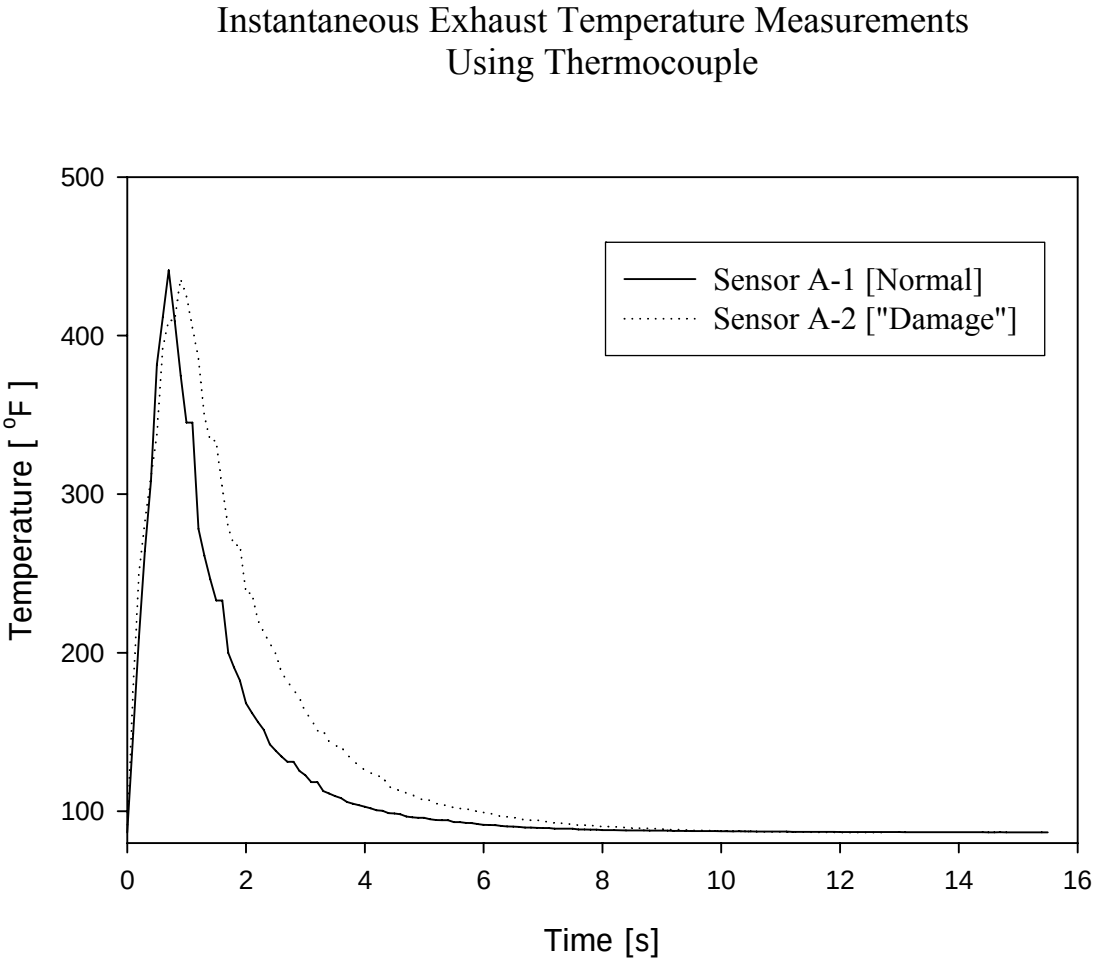

Figure 5-7: Instantaneous Exhaust Temperature Measure with Two Thermocouples

Sensor	Condition	Time Constant (msec)
A-1	Normal	136.4
A-2	Damage	136.9

Table 5-7: Time constant calculation

By observing the Table 5-7, the effect of damage in the thermocouple sensor as described in section 5.1.1 produced changes in the time constant. Sensor A-1 had initially a time constant of 0.041 sec when undamaged. After applying damage, sensor A-2, the time constant varied 0.4 percent.

In addition to this experiment, a thermocouple in which damage was introduced by variations in its temperature well was also examined. Here damage was introduced to sensor B-2 by the separation or lack of well contact and sensor B-3 was damaged covering the surface with paint. Figures 5-8 and Table 5-8 show the response and time constant calculations.

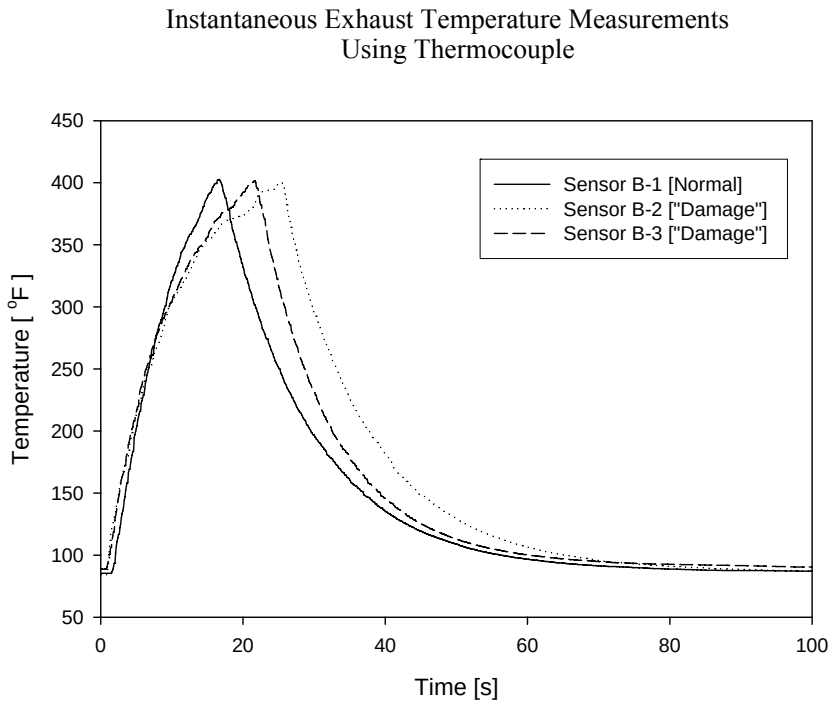

Figure 5-8: Instantaneous Exhaust Temperature Measurements Using Thermocouples

Sensor	Condition	Time Constant (sec)
B-1	Normal	0.359
B-2	Damage	0.381
B-3	Damage	0.373

Table 5-8: Time constant calculations

As seen from the Table 5-8, sensor B-1 had initially a time constant of 0.359 sec when undamaged. After applying damage in sensors B-2 and B-3, the time constant varied 6.1% and 3.9% respectively. These cases were performed at a constant velocity of 355 ft/min. As seem from these results, the use of examining the time constant as a means to detect anomalies is again promising.

6 Neural Network Implementation

This chapter deals with the analysis and classification of the experimental measurements from the previous chapter. A brief introduction to neural network (NN) theory is discussed. Several types of NNs are mentioned and the selection of the probabilistic neural network (PNN) is discussed. Later, a normal sensor with multiple damages scenarios is examined to check the NN performance in fault detection and classification.

6.1 Background

Neural networks (NNs) are suitable for pattern classification and information processing tasks. NNs are computational models composed of many simple and highly interconnected processing elements that process information and establish complex and highly nonlinear relationships and associations from large sets of data. When NNs are used, the data is required. Modeling produces an inverse relation and a solution to a direct problem, G. X. Ritter et. al. (1998). The advantage of using NNs in general is their capacity to clasiffy, even when trained with partially inaccurate data. In addition, some networks can continue learning and to improve their performance when presented with new training data.

A NN contains processing elements or neurons that have interconnection weights between themselves. These weights determine the nature and the type of connection between the neurons. A neuron with a single input vector is shown in Figure 6.1. The individual element inputs p_1 , p_2 ,… p_R are multiplied by weights $w_{1,1}$, $w_{1,2}$,… $w_{1,R}$ and the

weighted values are fed to the summing junction. Their sum is noted as Wp. The product of the matrix W and the input vector p is given by $[n]=[P]*[W]+[b]$.

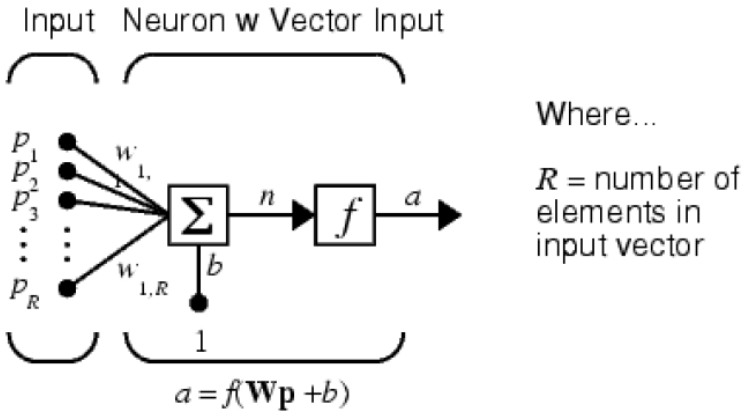

Figure 6-1: NN Diagram

The neuron has a bias *b*, which is summed with the weighted inputs to form the net input *n*. This sum, *n*, is the argument of the transfer function *f*, which produces the scalar output *a*. Note that *w* and *b* are both adjustable parameters of the neuron. Such parameters can be adjusted so that the network exhibits some desired behavior. Two or more of the neurons shown in Figure 6.1 can be combined in a layer, and a particular network could contain one or more such layers.

The overall methodology of using NNs is divided into two parts: the training stage; and the simulation stage. In the training stage, the network of interconnected neurons is presented with a set of input data and corresponding target output values. Then the interconnection weights among neurons and biases are iteratively adjusted, using

predefined learning rules, so the NN can replicate the target output values with minimum error. The training algorithms direct how the weights and biases change in response to a given input and output pair during the training stage. All of these algorithms use a gradient based technique called back propagation, which involves updating the network weights and biases in the direction in which the error between the outputs and targets decreases most rapidly (the negative of the gradient). The knowledge learned by NNs is represented by the connection weights.

6.2 Neural Network Selection

In order to find the most effective NN for damage detection and predictions, different NNs were examined. For example perceptrons are especially suited for simple problems in pattern classification but they have several limitations. The most important is that perceptrons can only classify linearly separable sets of vectors. If a straight line or a plane can be drawn to separate the input vectors into their correct categories, the input vectors are linearly separable. If the vectors are not linearly separable, learning will never reach a point where all vectors are classified properly.

Hopfield networks can act as error correction or vector categorization networks. Input vectors are used as the initial conditions to the network, which recurrently updates until it reaches a stable output vector. Hopfield networks are interesting from a theoretical standpoint, but are seldom used in practice. Even the best Hopfield designs may have false stable points that lead to incorrect answers. More efficient and reliable error correction techniques, such as back propagation, are available.

Radial basis networks are statistical based models. These NNs require more

neurons than standard feed forward back propagation networks, but often they can be designed in a fraction of the time it takes to train standard feed forward networks. One of the designs of radial basis networks is the probabilistic neural network (PNN), which combines some of the best attributes of statistical pattern recognition and feed forward neural networks. The PNN features very fast training time, offers robustness to noisy data and guaranteed convergence to a Bayesian classifier provided that enough training data is given. The architecture of the PNN is shown in Figure 6.2. It has a radial basis layer and a special competitive layer. When an input is presented, the first layer computes distances from the input vector to the training input vectors, and produces a vector whose elements indicate how close the input is to a training input.

The second layer (the competitive layer) sums these contributions for each class of inputs to produce as its net output a vector of probabilities. Finally, the "*compete*" transfer function on the output of the second layer picks the maximum of these probabilities, and produces a "1" for that class and a "0" for the other classes. Due to the advantages mentioned, a PNN based on radial basis networks was chosen for the implementation. All the PNNs used in this project were designed using the MATLAB® neural network toolbox.

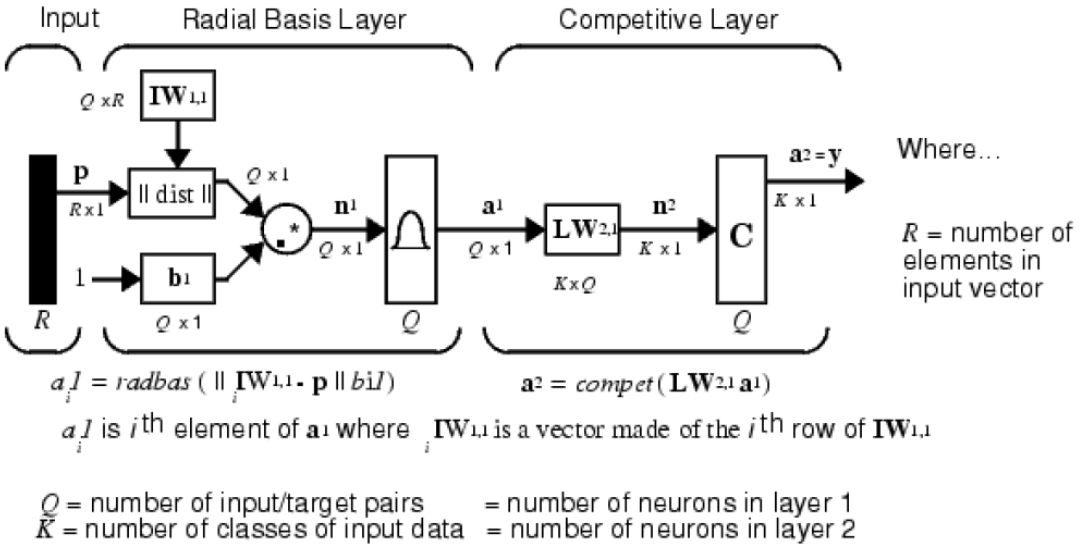

Figure 6-2: PNN Architecture

A novel class of artificial neural networks called, morphological associative memories (MAMs) were studied, G. X. Ritter et. al. (1998). They have the capability to retrieve complete stored patterns from noisy or incomplete input pattern keys. In MAMs the operations of multiplications and addition performed in the theory of NNs are replaced by addition and maximum (or minimum) of sums, respectively. The network weights are computed directly from the input/output values. Therefore convergence problems do not exist in this kind of networks. A MAM network and a PNN were compared based on their performance in recognizing noisy data. According to the obtained results, PNNs showed to be more efficient than MAMs when the noisy data was present.

All the previous mentioned NNs are not designed to be incremental learners since old examples are represented explicitly in the networks. Every new example demands the

modification of the network architecture by the addition of another pattern unit and associated connections. However once the NNs were properly trained, the weights and biases do not need to be recalculated when the network is used to classify a new input pattern.

The basic flow diagram to design a PNN is depicted in the next figure.

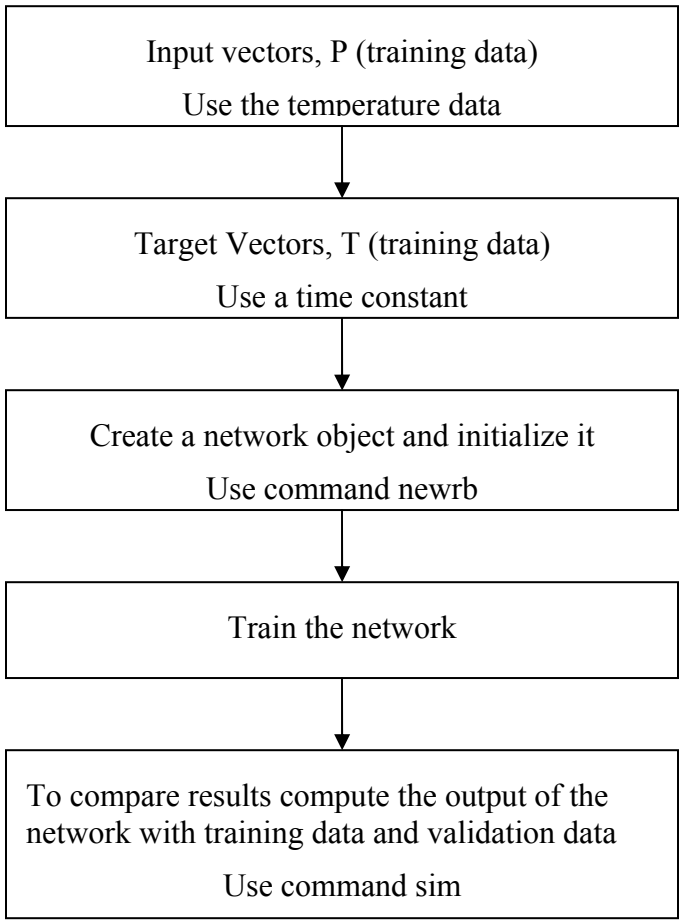

Figure 6-3: Basic flow diagram to design a neural network

The data required for training the NNs is provided by experimental results. This information is preprocessed using MATLAB® routines. The preprocessing of the data involves two main stages: First the extraction of synthetic features related to the presence and the characteristics of the damage and second, the normalization of the input patterns to improve convergence of the learning rule.

6.3 Experimental Study Using Neural Networks

The algorithm mentioned in chapter 4 has been used to characterize transient thermocouples data. In this section we will use a NN based algorithm to identify anomalies present in the temperature sensors. The simplest case of testing a NN involves classifying one of the training patterns and verifying that it has correctly associated it with the corresponding target.

In a real case of an aircraft engine, typical scenarios can affect the measurement of temperature using sensors. These include impact (birds, ice), fatigue, corrosion and drift to mention a few. As a result of these occurrences, temperature readings may not be accurate.

The NNs scheme of Figure 6.4 was trained using the data from damage sensors listed in Table 6.1. These training cases correspond to simple damage scenarios of experimental case 1 of chapter 5.

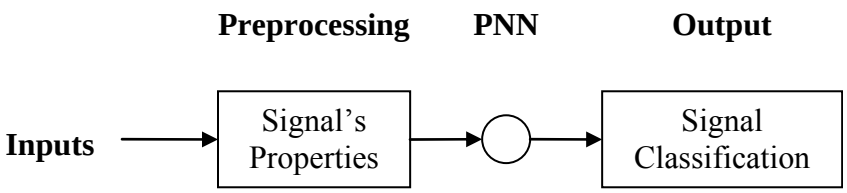

Figure 6-4: NN scheme for thermocouple data classification

Figure 6-1 shows the scenarios of the thermocouple with a protective sheath.

Sensor value	Thermocouple Type K with different bulbs	Undamaged Case	Damage Type
B1		Welded joint with contact well	N/A
B2		N/A	Welded joint without contact well
B3		N/A	Painted probe

Table 6-1: Training Cases: Undamaged and Damage Scenarios

In order to train the NN, the data that come from the graph of Figure 6-5 was used to make the input matrix [P].

$$P = \begin{bmatrix} B1_{1,1} & B2_{1,2} & B3_{1,3} \\ B1_{2,1} & B2_{2,2} & B3_{2,3} \\ B1_{n,1} & B2_{n,2} & B3_{n,3} \end{bmatrix}$$

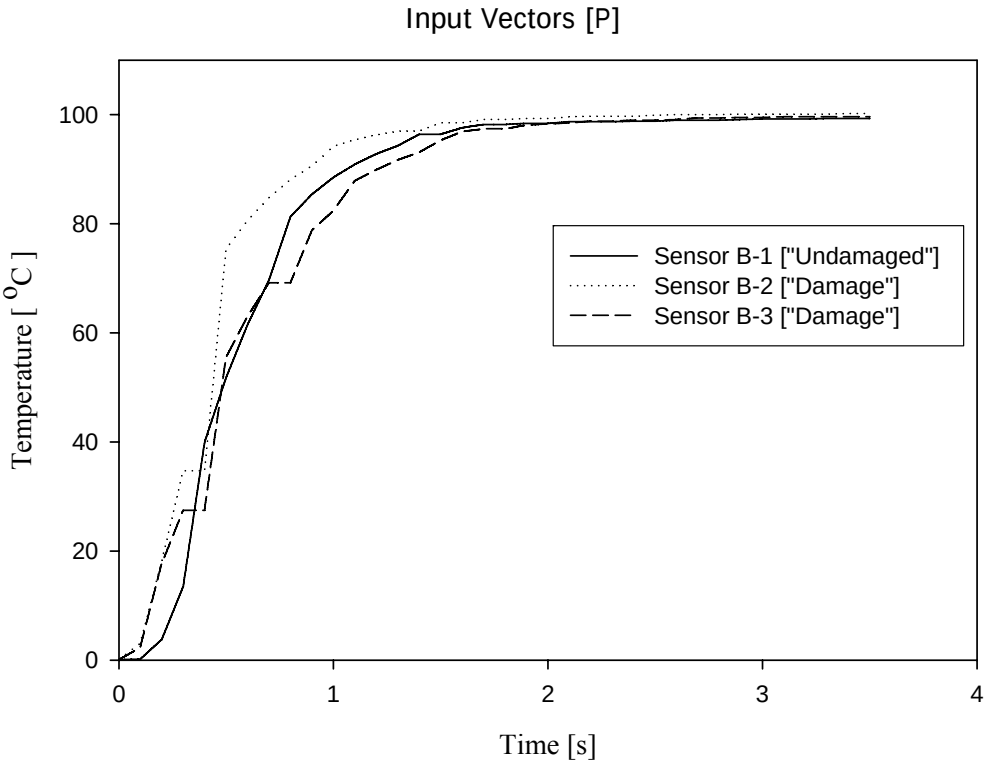

Figure 6-5: Data used to determine input vectors, [P] for tanning the NN system

The temperature response of each sensor with undamaged and damaged scenarios was characterized by a time constant set. In this case a unique PNN in a Radial basis NN structure was used for a curve classification as depicted in the process of Figure 6-4. Each time constant of the test case, Figure 6-6, was compared with contour data and classified as normal or damaged. This classification is based on numerical cases learned in section 6.2. The input vectors [T] were determined with time constant data that was obtained by the algorithm. Figures 6-6 show the time constant calculation using the algorithm.

$$T = \begin{bmatrix} \tau_{B1} & \tau_{B2} & \tau_{B3} \end{bmatrix}$$

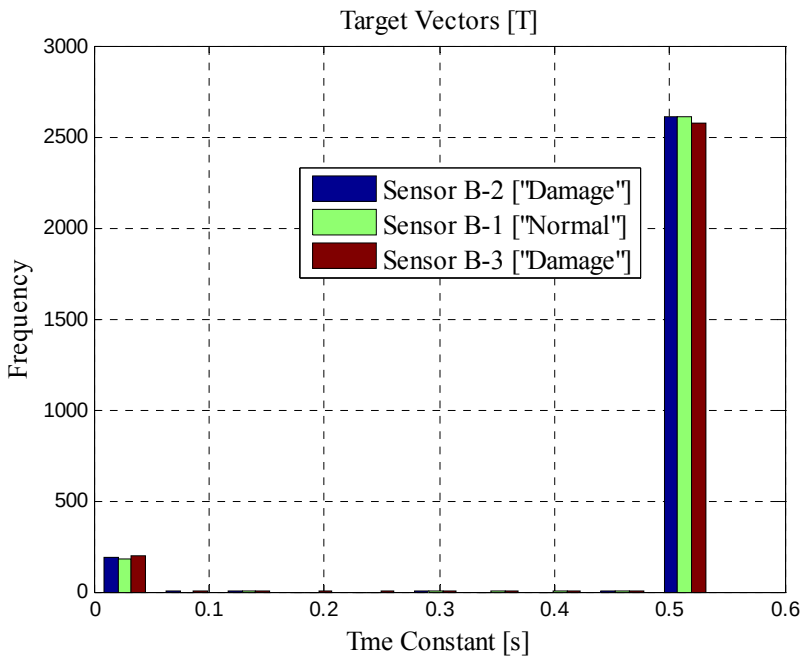

Figure 6-6: Target vectors, [T] for training the NN system

Here several test cases were chosen to check the performance of the proposed Radial basis NN architecture in damage detection. The MATLAB command *newrb*, was used to create a Radial basis neural network and is given in equation 6-1.

$$net = newrb(P, T, GOAL, SPREAD) \qquad 6\text{-}1$$

Here

P: is an input vectors that represents the temperature data

T: is target class vector that represents the time constant data

GOAL: is mean squared error goal, default = 0.0.

SPREAD: is spread of radial basis functions, default = 1.0.

The function *newrb* takes matrices of input and target vectors, P and T, and design parameters "GOAL" and, "SPREAD", and returns the desired network. The function *newrb* iteratively creates a radial basis network one neuron at a time. Neurons are added to the network until the sum-squared error falls beneath an error goal or a maximum number of neurons have been reached.

The time constant estimated by the algorithm (target vector T) and the output of the Radial basic network can now be compared. Table 6-2 shows the performance of the network.

Table 6-2: Neural Network performance

	Time Constant (sec)		
Sensor	**B1**	**B2**	**B3**
Neural Network estimation	0.5009	0.4903	0.5402
Actual Value	0.5000	0.4900	0.5400
Error (%)	**0.18%**	**0.06%**	**0.04%**

By examining Table 6-2 it can be observed that the network structure approximates the time constant or the target vectors [T]. The error was very close to zero. These obvious results suggest that the priory NN was properly trained. The convergence values used are mean square error (GOAL=0.02) and the spread value (SPREAD=0.1).

After the N.N. was trained, a new scenario was selected for classification. The damage sensor consists of two dissimilar wires material with a twisted joint covered with

a sheath. A thermocouple data of the new scenario is given in appendix A-2. The result from the neural network classification is show in Table 6-3.

Table 6-3: Sensor classification

New sensor scenario for classification			
	Time Constant (sec)	**Condition**	**Classification**
Neural Network estimation	0.492	Damage	The N.N. associates the damage with the sensor B-2 as shown in Table 6-4
Actual Value	0.481		

If you compare the classification results of Table 6-3 and the NN estimation as depicted in Figure 6-2, it can be easily observed that the NN successfully classified the test case with respect to the training data. The neural network produces a “1” for that class and a “0” for the other classes and associated the damage with the sensor B-1 as depicted in Table 6-1.

7 Conclusions

This investigation developed an algorithm capable of measuring the time constant of a thermocouple using transient data. The algorithm is restricted to signals in which the sensor time constant is at least an order of magnitude faster than the transient of the system. In addition, only signals that can be constructed using a piecewise ramp functions can be used. Since time derivatives are taken in the procedure, noisy signals can produce significant errors. This effect however can be reduced to acceptable values by application of a moving average filter.

The technique was corroborated experimentally for various sensors with different time constants using different input signals to verify the algorithm. In every case studied, the algorithm determined the time constant with the largest error being less than five percent. By modifying sensors, (painting, adding mass etc) time constant variations were created. The technique was capable of detecting changes as small as two percent.

To examine the applicability of the algorithm, an experimentally validated ANN to detect anomalies in temperature sensors was also developed. A radial basis PNN architecture proved to be the most efficient architecture for anomaly detection and sensor modification classification The technique has contributed to the current state of sensor anomaly detection. Schemes used by industry usually use steady state techniques and/or statistical means for sensor evaluation. This technique uses transient data and can establish a virtual model of the sensor. This capability can be used in control and determination algorithms and is not currently available or used in today's gas-turbine anomaly detection schemes.

8 References

Brotherton Tom, Mahey Ryan: "Anomaly Detector Fusion Processing for Advanced Military Aircraft", Proceeding of the IEEE Aerospace Conference, Big Sky Montana, March 2001, pp.1-13.

Chatterjee Santanu, Litt Jonathan S.: "Online Model Parameter Estimation of Jet Engine Degradation for Autonomous Propulsion Control", N&R Engineering Corporation and U.S. Army Research Laboratory, Glenn Research Center, Cleveland, Ohio, October 2003, pp. 1-22

C. M. Bishop, Neural Networks for Pattern Recognition, OXFORD University Press, NY, 2004.

Colin Mercer: "Data Smoothing: RC Filtering and Exponential Averaging", Prosig Signal Processing Tutorials, visit Prosig at www.prosig.com, 28 april 2003, pp. 1-3.

Dimitry Gorinevsky, Emmanuel Nwadiogbuy, Dinkar Mylaraswamy: "Model-based Diagnostics for Small-scale Turbomachines", Honeywell International 41st IEEE CDC Las Vegas, NV, December 10-13, 2002, pp. 1-6.

Doebelin Ernest O., "Measurement Systems, Application and Design", McGraw-Hill Book Company, New York, 1983, pp. 99-120.

Dorr Richard and Kratz Frederick: "Detection, Isolation, and Identification of Sensor Faults in Nuclear Power Plants", Paper: IEEE Transaction on Control System Technology, Vol. 5, No. 1, January 1997, pp. 42-60.

Figliola Richard S. and Beasley Donald E.: "Theory and Design for Mechanical Measurements", Third edition, John Wiley & Sons, Inc, USA, 2000, pp. 283-343.

Frith Peter and Karvounis George: "Model-Based Decision Support Tools For T700 Engine Health Monitoring", Airframes & Engines Division, DSTO, DSTO-HUMS2001, CDROM, Paper 5-12, pages 1-12.

Greitzer, Frank L. and Pawlowski, Ronald A.: "Embedded Prognostics Health Monitoring", Pacific Northwest National Laboratory, Paper Presented at International Instrumentation Symposium, Embedded Health Monitoring Workshop, PNNL-SA-35920 May - 2002, pp. 1-10.

Hung P.C., Irwin G. Kee R.: "Difference equation approach to two-thermocouples sensor characterization in a constant velocity flow environments", American Institute of Physics, Review of Scientific Instruments ***76***, 024902, 2005, pp. 1-10.

Katsuhiko Ogata: “System Dynamics”, Second Edition, Prentice Hall, Inc, 1992, pp. 379-387

Kobayashi Takahisa and Simon Donald L.: “A Hybrid Neural Networks-Genetic Algorithm Technique For Aircraft Engine Performance Diagnostics”, Prepared for the 37th Joint Propulsion Conference and Exhibit, AIAA, ASME, SAE, and ASEE, Salt Lake City, Utah, July 8–11, 2001, pp.1-16.

Link C. Jaw, Dong N. Wu: “Anomaly Detector and Reasoning with Embedded Physical Model”, Scientific Monitoring, Inc., Tempe, Arizona, U.S.A., IEEE, 2002, pp. 1-9.

LiJie Yu, D.J. Cleary and P.E. Cuddihy: “A Novel Approach to Aircraft Engine Anomaly Detection and Diagnostics”, General Electric Global Research Center, Article for 19th Conference on Uncertainty in Artificial Intelligence, April 2003, pp. 1-12.

Luo, Jianhui, Namburu Madhavi, Pattipati Krishna, Qiao Liu, Kawamoto Masayuki and Chigusa Shunsuke: “Model-based Prognostic Techniques”, Dept. of ECE, University of Connecticut & Toyota Technical Center U.S.A, IEEE Autotestcon 2003 Conference, September 22-25,2003 pp. 1-11.

Mattern, Duane L., Ten-Huel, Graham, Ronald, McCoy, William: “Using Neural Networks for Sensor Validation”, NASA Center for Aerospace Information, Lews Research Center, Articule for 34th Joint Propulsion Conference, Clevelad, Ohio, July 1998, pp. 1-16.

MATLAB® Neural Network Toolbox Version 4.0.1 Release 12.1. http://www.mathworks.com/access/helpdesk/help/toolbox/nnet/.

Neophytos Chiras, Ceri Evans and David Rees: “Nonlinear Gas Turbine Modeling Feed-forward Neural Networks”, GT-2002-30035, ASME Turbo Expo 2002,Amsterdam, The Netherlands, June 3-6, 2002, pp. 1-8.

Ortiz, J. L, Parsiani, H., and Tolstoy, L., University of Puerto Rico at Mayagüez. Application of Morphological Associative Memories and Fourier Descriptors for Recognition of Noisy Subsurface Image.

Pirinen T.W.: “Detection and Compensation of Sensor Malfunction in Time Delay Based Direction of Arrival Estimation”, International Computer Science Institude (ICSI) 1947 Center St., Berkeley, CA, USA, 2004 IEEE, pp. 1-4.

Penwell, Roy: “System Trace: Real Time Monitoring for Embedded System Development and Operation”, Miamisburg, OH 45342, ITCN, Topic number: N98-160.

Ritter, G. X., Sussner, P. and Diaz de Leon, J. L., 1998 IEEE Transaction on Neural Networks 9(2), 281-293. Morphological Associative Memories.

Roemer Michael J.and Kacprzynski Gregory J.: “Advanced Diagnostics and Prognostics for Gas Turbine Engine Risk Assessment”, IGTI/ASME Turbo Expo, Munich, Germany, May 2000, pp. 1-10

Shapiro H, Moran M.: “Fundamentals of Engineering Thermodynamics”: John Wiley & Sons, Inc., New York, 4th ed., pp. 440-475.

Simani S., Fantuzzi C., Beghelli S.: “Diagnosis Techniques for Sensor Faults of Industrial Processes”, IEEE Transaction on Control System Technology, Vol. 8, No. 5, September 2000, pp. 848-855.

Steven W. Smith, Ph.D: “The Scientific Engineer’s Guide to Digital Signal Processing”, California Technical Publishing, San Diego, CA, www.dspguide.

Steven R, Gould: Engineering Statistics Handbook, Chapters 6.4.3.1, 6.4.3.3, http://www.itl.nist.gov/div898/handbook/pmc/section4/pmc43.htm

Suresh Sampath and Riti Singh: “Computational Intelligence for Diagnosing Gas path related faults in Gas Turbine Engines”, School of Engineering, Cranfield University, Bedfordshire. MK 43 OAL.UK, CiteSeer.IST, 2002, pp. 1-19.

Tao XU and Qi Wang: “Application of MSPCA to sensor Fault Diagnosis”, Department of Automatic Test and Control, Harbin Institute of Technology, Harbin, Vol. 32, No. 3, May 2006., pp. 417-421.

Tobias Randall D.: “An-Introduction to Partial Least-Squares Regression”, SAS Institute Inc., Cary, NC, pp. 1-8.

Tumer, Irem Y.: “Anomaly Detection & Failure Prediction in Anomaly Detection & Failure Prediction in Aerospace Vehicles: Modeling of Variability for Vehicle Monitoring Systems”, Computational Sciences Division, NASA Ames Research Center Conference, Monterey, CA, September 2002, pp. 1-9.

Wang S. and Wang J.: “Robust sensor fault diagnosis and validation in HVAC systems”, Department of Building Services Engineering, The Hong Kong Polytechnic University, Kowloon, Hong Kong, The Institute of Measurement and Control, (2002) pp. 231-262

Zhao J., Ivan J. N. and DeWolf J. T., 1998 Journal of Infrastructure Systems 4, 93-101. Structural Damage Detection Using Artificial Neural Networks.

Appendix A

Appendix A-1: Thermocouple Data

Thermcouple data	
time (sec)	Temperature (^{o}C)
0.000	0.100
0.063	0.163
0.125	1.100
0.188	3.350
0.250	8.650
0.313	16.813
0.375	33.375
0.438	44.425
0.500	51.800
0.563	57.863
0.625	63.550
0.688	68.675
0.750	75.500
0.813	81.813
0.875	84.375
0.938	86.563
1.000	88.500
1.063	90.000
1.125	91.375
1.188	92.563
1.250	93.550
1.313	94.563
1.375	95.875
1.438	96.400
1.500	96.400
1.563	97.150
1.625	97.750
1.688	98.125
1.750	98.200
1.813	98.225
1.875	98.350
1.938	98.400
2.000	98.400

time (sec)	Temperature (^{o}C)
2.063	98.588
2.125	98.700
2.188	98.700
2.250	98.700
2.313	98.713
2.375	98.775
2.438	98.800
2.500	98.800
2.563	98.925
2.625	99.000
2.688	99.000
2.750	99.000
2.813	99.012
2.875	99.075
2.938	99.138
3.000	99.200
3.063	99.200
3.125	99.200
3.188	99.200
3.250	99.250
3.313	99.300
3.375	99.300
3.438	99.300
3.500	99.300

Appendix A-2: New scenario thermocouple data

A new scenario selected for NN classification. The damage sensor consists of two dissimilar wires material with a twisted joint covered with sheath

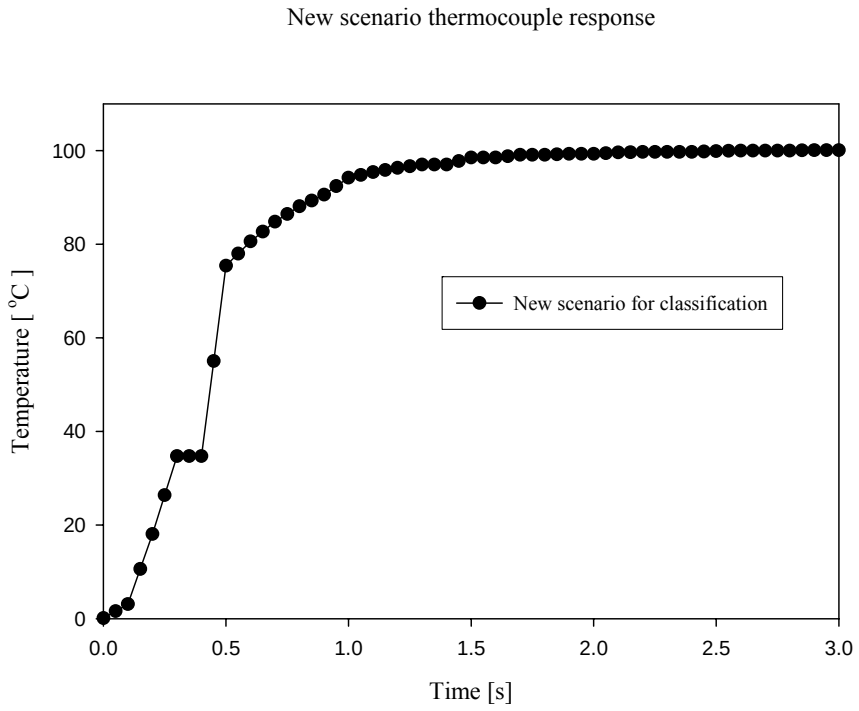

Appendix A-3: Filters Theory

Moving Average Filter (M.A.F.)

The moving average is the most common filter in Digital Signal Processing (DSP), mainly because it is the easiest digital filter to understand and use. The moving average filter is optimal for a common task: reducing random noise while retaining a sharp step response, Steven W Smith. This makes it the premier filter for time domain encoded signals. The moving average is the worst filter for frequency domain encoded

signals, with little ability to separate one band of frequencies from another.

The moving average filter operates by averaging a number of points from the input signal to produce each point in the output signal. In equation form, this is written:

$$y[i] = \frac{1}{M} \sum_{j=0}^{M-1} x[i+j] \qquad 0\text{-}1$$

Where x[ ] is the input signal, y[ ] is the output signal, and M is the number of points used in the moving average.

It is optimal for a common problem, reducing random white noise while keeping the sharpest step response.

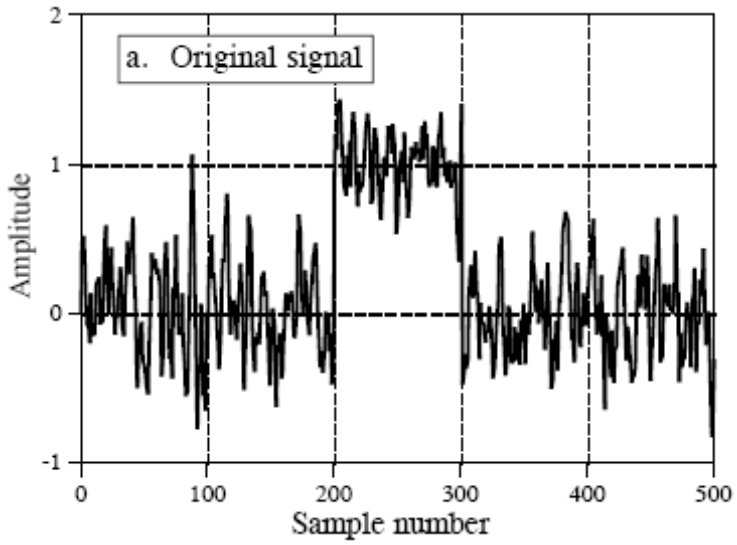

Rectangular pulse signal with a random noise

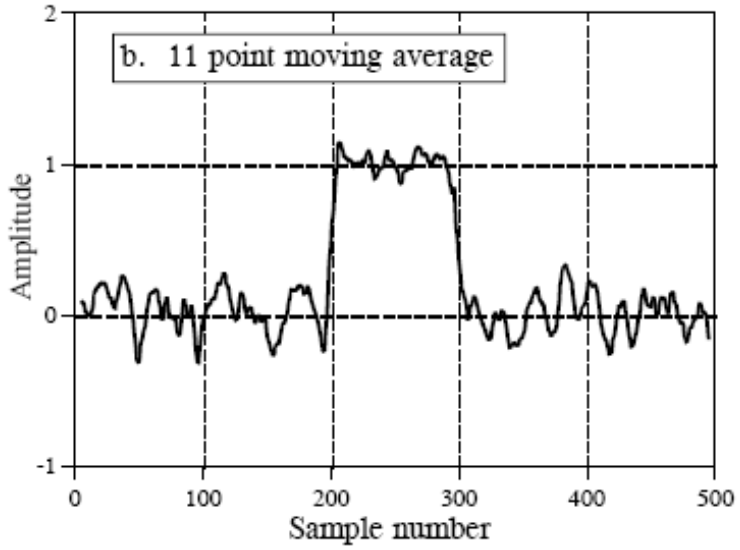

Filtered signal with 11 point moving average filters

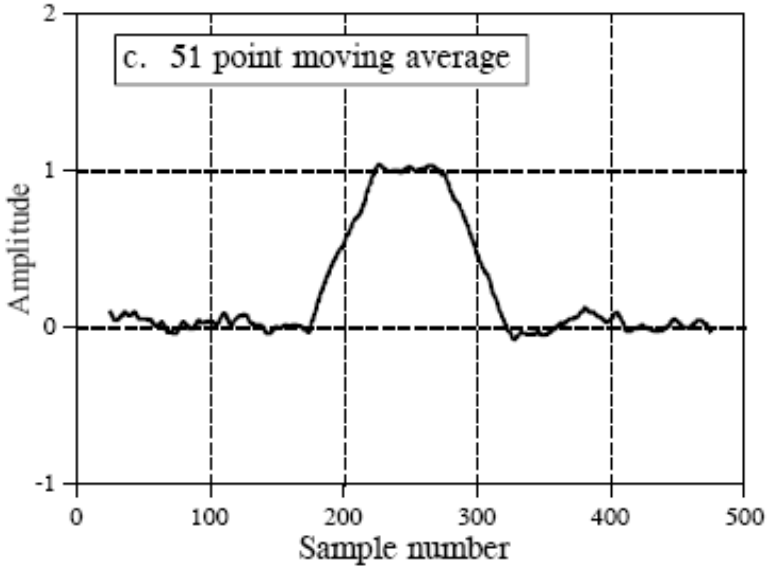

Filtered signal with 51 point moving average filters

The signal in (a) is a pulse buried in random noise. In (b) and (c), the smoothing

action of the moving average filter decreases the amplitude of the random noise (good), but also reduces the sharpness of the edges (bad). The moving average filter is the optimal solution for this problem, providing the lowest noise possible for a given edge sharpness.

Exponential Average Filter (E.A.F.)

This smoothing scheme begins by setting f_2 to Y_1, where f_k stands for smoothed observation, and y stands for the original observation. The subscripts refer to the time periods, 1, 2,…, n. For the third period, f_3 = alpha * Y_2 + (1-alpha) * f_2; and so on. There is no S1; the smoothed series starts with the smoothed version of the second observation, Steven R, Gould.

It takes a fraction of the current input and one minus this fraction times the previous output. Algebraically at time k the smoothed output f_k, for any time period t, the smoothed value f_k is found by computing:

$$f_k = \alpha Y_k + (1-\alpha) f_{k-1} \qquad \text{0-2}$$

Where $0 < \alpha < 1$

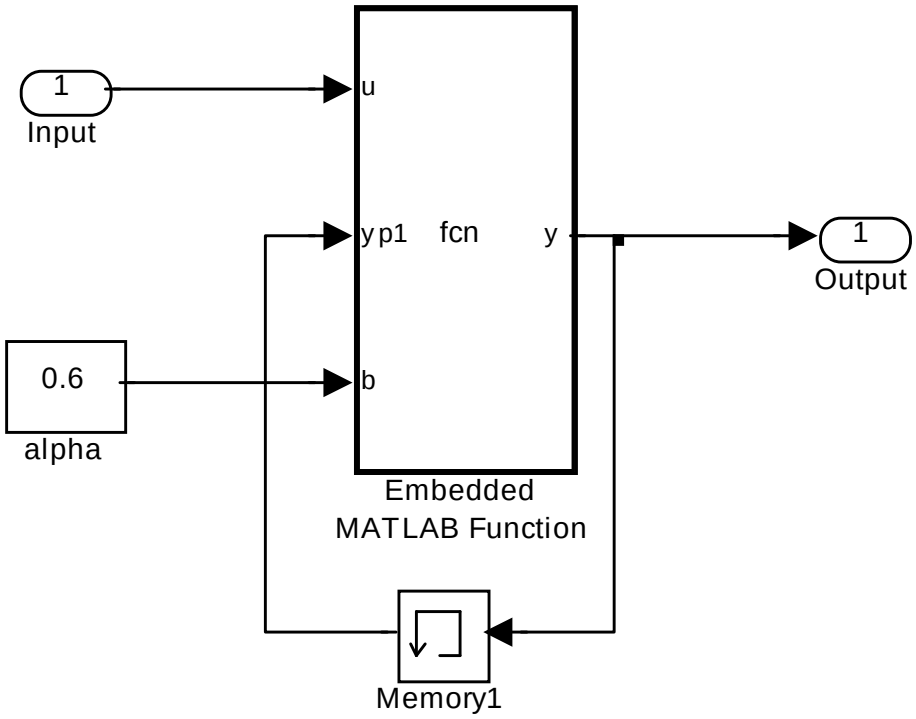

Exponential Average Filter Simulink-Model

Exponential Average Smoothed Filter (E.A.S.F.)

Exponential smoothing average also known as double exponential smoothing is a refinement of the popular simple exponential smoothing model but adds another component which takes into account any trend in the data. Simple exponential smoothing models work best with data where there are no trend or seasonality components to the data, Steven R, Gould. When the data exhibits either an increasing or decreasing trend over time, simple exponential smoothing tend to lag behind observations. Double

exponential smoothing is designed to address this type of data series by taking into account any trend in the data. As with simple exponential smoothing, in double exponential smoothing models past observations are given exponentially smaller weights as the observations get older. In other words, recent observations are given relatively more weight in forecasting than the older observations.

There are two equations associated with Double Exponential Smoothing:

$$f_t = \alpha * Y_t + (1-\alpha) * (f_{t-1} + b_{t-1}) \qquad 0\text{-}3$$

$$b_t = \gamma * (f_t - f_{t-1}) + (1-\gamma) * b_{t-1} \qquad 0\text{-}4$$

Where:

Y_t - is the observed value at time t.

f_t - is the forecast at time t.

b_t - is the estimated slope at time t.

α - Representing alpha - is the first smoothing constant, used to smooth the observations.

γ - Representing gamma - is the second smoothing constant, used to smooth the trend.

The first smoothing equation adjusts f_t directly for the trend of the previous period, b_{t-1} by adding it to the last smoothed value, f_{t-1}. This helps to eliminate the lag and brings f_t to the appropriate base of the current value. The second smoothing equation then updates the trend, which is expressed as the difference between the last two values. The equation is similar to the basic form of single smoothing, but here applied to

the updating of the trend. To initialize the double exponential smoothing model, f_1 is set to Y_1, and the initial slope b_1 is set to the difference between the first two observations; i.e. $Y_2 - Y_1$. The smoothing constants must be values in the range 0.0 - 1.0. The "best" value to use for the smoothing constants depends on the data series being modeled. The speed at which the older responses are dampened (smoothed) is a function of the value of the smoothing constant, Steven R, Gould. When this smoothing constant is close to 1.0, dampening is quick (more weight is given to recent observations) and when it is close to 0.0, dampening is slow and relatively less weight is given to recent observations.

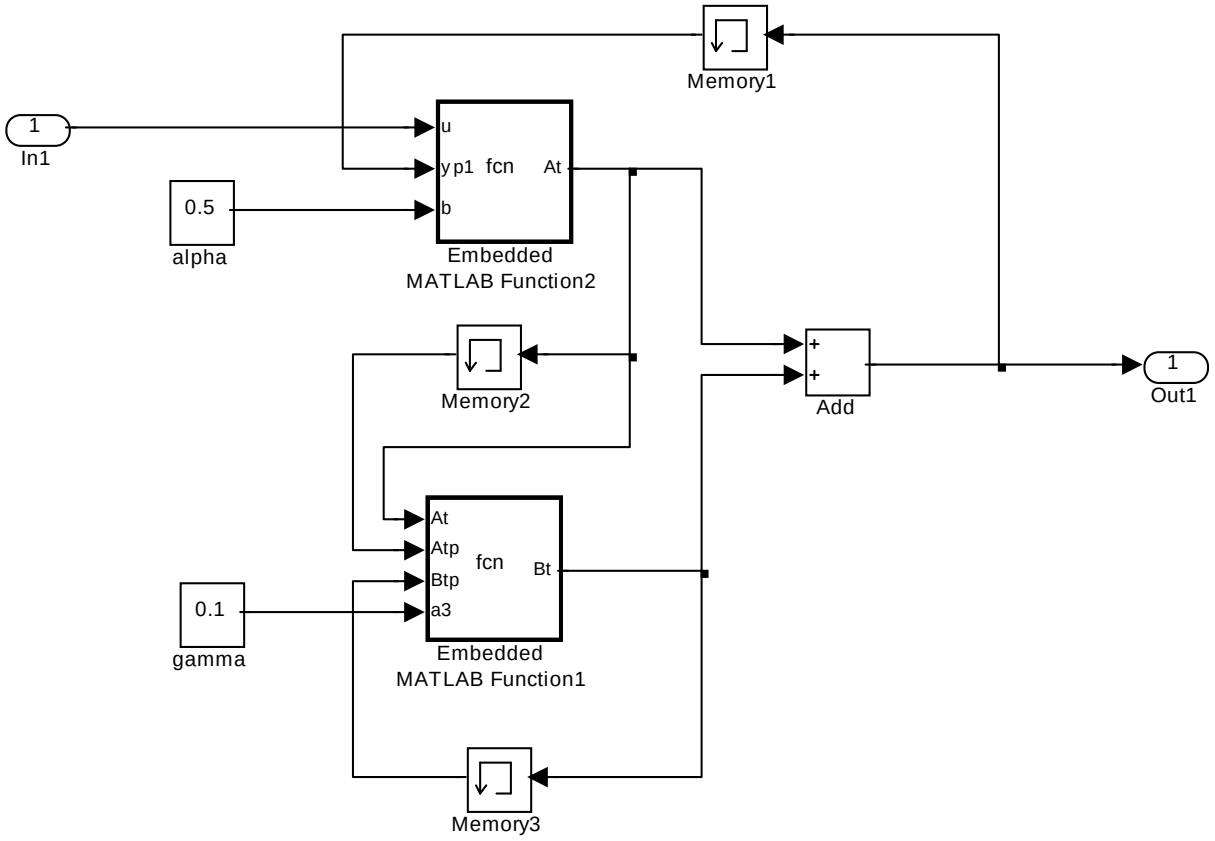

Exponential Average Smoothed Filter Simulink-Model